AD-A120 410 IMAGE RECONSTRUCTION USING LARGE OPTICAL TELESCOPES(U) 1/2
STEWARD OBSERVATORY TUCSON ARIZ E K HEGE ET AL.
15 FEB 82 AFGL-TR-82-0136 F19628-78-C-0058

UNCLASSIFIED F/G 20/6 NL

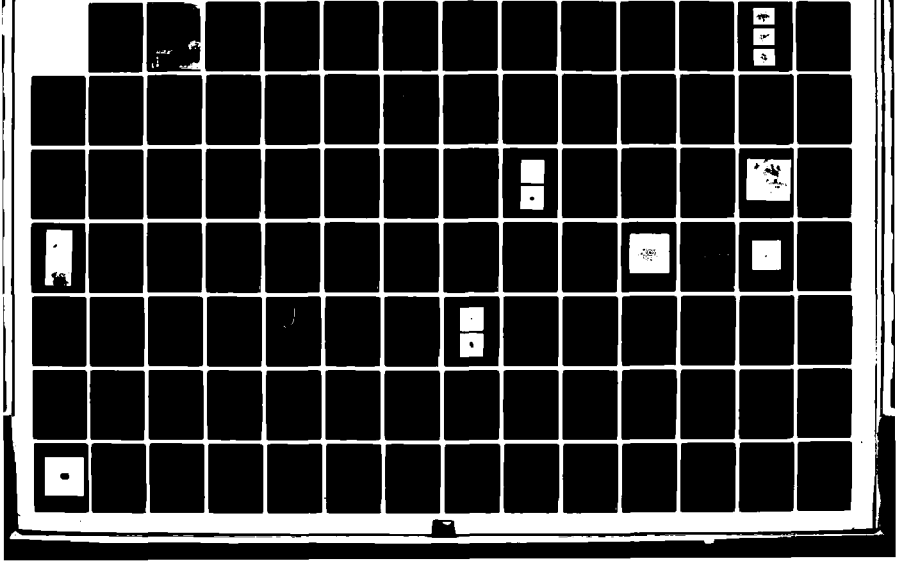

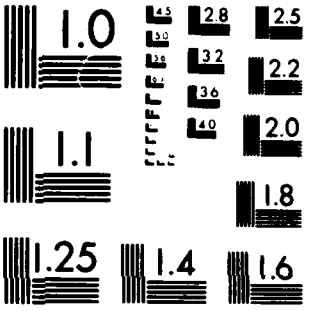

MICROCOPY RESOLUTION TEST CHART
NATIONAL BUREAU OF STANDARDS 1963-A

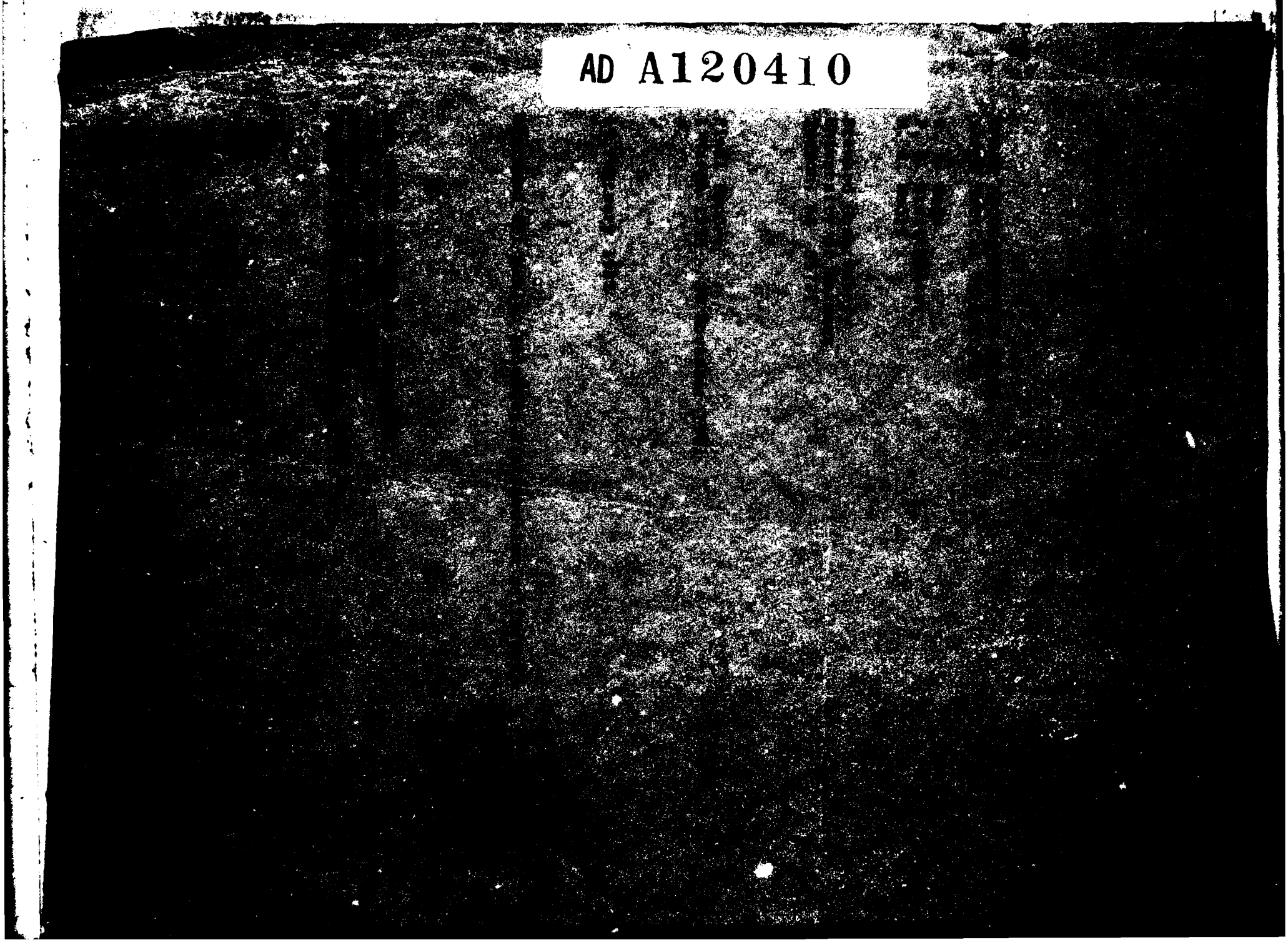

Unclassified

SECURITY CLASSIFICATION OF THIS PAGE (When Data Entered)

REPORT DOCUMENTATION PAGE		READ INSTRUCTIONS BEFORE COMPLETING FORM
1. REPORT NUMBER AFGL-TR-82-0136	2. GOVT ACCESSION NO. AD-A120 410	3. RECIPIENT'S CATALOG NUMBER
4. TITLE (and Subtitle) IMAGE RECONSTRUCTION USING LARGE OPTICAL TELESCOPES		5. TYPE OF REPORT & PERIOD COVERED Final Report 1 Mar 1978 - 30 Nov 1981
		6. PERFORMING ORG. REPORT NUMBER
7. AUTHOR(s) E.K. Hege P.A. Strittmatter N.J. Woolf		8. CONTRACT OR GRANT NUMBER(s) F19628-78-C-0058
9. PERFORMING ORGANIZATION NAME AND ADDRESS Steward Observatory University of Arizona Tucson, Arizona 85721		10. PROGRAM ELEMENT, PROJECT, TASK AREA & WORK UNIT NUMBERS 61102F 2311G3AM
11. CONTROLLING OFFICE NAME AND ADDRESS Air Force Geophysics Laboratory Hanscom AFB, Massachusetts 01731 Monitor/Richard R. Radick/PHS		12. REPORT DATE 15 February 1982
		13. NUMBER OF PAGES 122
14. MONITORING AGENCY NAME & ADDRESS(if different from Controlling Office)		15. SECURITY CLASS. (of this report) Unclassified
		15a. DECLASSIFICATION/DOWNGRADING SCHEDULE

16. DISTRIBUTION STATEMENT (of this Report)

Approved forpublic release; distribution unlimited

17. DISTRIBUTION STATEMENT (of the abstract entered in Block 20, if different from Report)

18. SUPPLEMENTARY NOTES

19. KEY WORDS (Continue on reverse side if necessary and identify by block number)

Speckle_Interferometry
Image_Reconstruction
High-Resolution_Imaging
Atmospheric_Seeing
Detectors
Data_Reduction

This report covers

20. ABSTRACT (Continue on reverse side if necessary and identify by block number)

In 1977, photographic detectors were used to record speckle data. Photographic data are difficult to calibrate, have a low recording duty cycle, and are very cumbersome to reduce digitally for large numbers of frames. We have developed a digital television detector system with the capability to identify individual photon events. Using this system we have applied speckle techniques to objects fainter than +17 magnitude.

DD FORM 1 JAN 73 1473 EDITION OF 1 NOV 65 IS OBSOLETE

Unclassified

SECURITY CLASSIFICATION OF THIS PAGE (When Data Entered)

20. Abstract (Cont'd)

Fourier optical data reduction methods produced size and shape information only, accurate to about 30% for objects of size comparable to the telescope diffraction limit. We have developed data reduction and calibration methods that provide size and shape information accurate to better than 5% at the telescope diffraction limit, and have produced diffraction limited images for several targets.

By extending speckle techniques to accurate measurement of low surface brightness objects we have measured diameters for over a dozen asteroids and possibly detected binary systems, directly resolved and imaged the Pluto/Charon system, resolved a multiple QSO (quasar) and we have mapped and imaged asymmetries in the envelope around the supergiant star Alpha Orionis.

A principle objective of this program was to show the utility of speckle interferometry for studying Earth-orbital satellites. This task required developing pointing and tracking algorithms for satellite acquisition and tracking using conventional astronomical telescopes. We successfully accomplished this objective and produced the first optical resolution of a high orbit satellite, a Soviet Molniya.

Even the largest single mirror telescopes do not provide sufficient resolution for studying synchronous satellites, or to make detailed maps of stellar surfaces. We therefore, undertook a program to adapt and use the new Multiple Mirror Telescope (MMT), with an effective aperture of nearly 7 meters, for speckle interferometry. We have recently successfully combined separate MMT mirror beams to produce speckle results for stellar targets at the full 7 meter diffraction limit.

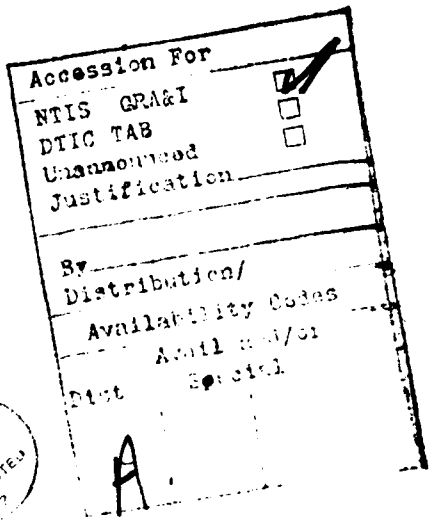

CONTENTS

List of Figures 6

List of Tables 7

I. Introduction: Why Speckle Interferometry? 8

I.A. Status of Speckle Interferometry in 1977. 12

I.B. Summary of Objectives Proposed and Results Achieved 13

I.C. Areas for Future Development 15

II. Speckle Interferometry at Steward Observatory 16

II.A. The Speckle Camera 17

II.B. The Digital Television System 19

II.C. Speckle Data Reductions 21

II.D. Further Complications and Solutions 23

II.D.1. Temporal Problems and Spatial Effects 23

II.D.2. Bias Effects 24

II.D.3. Signal-to-noise Effects 25

II.D.4. Instrumental Effects 26

II.E. An Earth Satellite Observation 28

II.F. Speckle Image Reconstruction 30

II.G. Speckle Interferometry with the Multiple Mirror Telescope (MMT) 35

III. Atmospheric Seeing and Speckle Interferometry 44

III.A. Effects of Dome Seeing 44

III.B. High Resolution Imaging from the Ground 44

III.C. Influence of Telescope and Atmospheric Distortions on Speckle Interferometry 46

III.C.1. Image Wander 47

III.C.2. Effect of Telescope Focus 57

III.C.3. Effect of Observing Bandpass 59

III.C.4. Effect of Exposure Time 62

III.C.5. Photon Statistics 64

IV. Scientific Results Obtained Using Speckle Interferometry 67

IV.A. The Triple Quasar 67

IV.B. Pluto/Charon 68

IV.C. Betelgeuse 68

IV.D. Asteroid Measurements 69

V. Speckle Interferometry for High Resolution Imaging of Earth-orbiting Satellites: Present Status and Future Prospects 71

V.A. Acquisition and Tracking of Non-sidereal Objects 73

V.A.1. Tracking Rate Requirements and Present Capabilities 73

V.A.2. Acquisition of Objects with Inaccurate Coordinates 75

V.A.3. Tracking Software for Telescope Drives 75

V.B. Real-time Data Capture and Reduction 78

V.B.1. Hardware Requirements 80

V.B.2. Software Requirements 80

V.B.3. Plan for System Improvements 81

V.C. Detector Resolution and Diffraction Limited Image Sampling 85

VI. Speckle Interferometry for Scientific Investigations 89

VI.A. Resolved Stellar Systems, Galactic Nuclei and QSO's 89

VI.B. Speckle Polarimetry 92

VI.C. Validation of Image Reconstruction Techniques 93

VI.D. Speckle Image Studies 94

VII. Abstracts of Publications 94

VIII. Speckle Interferometry Software: Summary of Computer Programs for Data Reductions and Image Analysis 113

VIII.A. Minicomputer Systems 113

VIII.B. Cyber 175/DEC 10 Systems 114

VIII.C. Image Analysis and Interpretation 116

IX. Acknowledgements 120

X. References 121

List of Figures

I.1. Specklegrams. 10

II.1. The speckle camera. 18

II.2. The digital television system. 20

II.3. Instrumental effects 27

II.4. Reconstructed images. 34

II.5. The coherent beam combiner. 36

II.6. Interference fringes for point source. 38

II.7. Interference fringes for binary star. 40

II.8. Power spectrum of α Tau. 42

III.1. PG 1115+080. 50

III.2. Tracking record. 51

III.3. Pluto. 52

III.4. MTF for MMT interferometer. 54

III.5. Effect of telescope focus. 58

III.6. Effect of observing bandwidth. 60

III.7. Effect of anti-dispersion prisms. 61

III.8. Effect of exposure time. 63

V.1 Seeing-corrected power spectrum from event centroided data. 82

VIII.1 Summary of data reductions processes. 117

List of Tables

III.I.	Image Wander	48
III.II.	Predicted Effect of Seeing on Interferometric Contrast	56
V.I.	Satellite Resolution Limits	71
V.II.	Satellite Rates	74
VIII.I.	Software (FORTH)	117
VIII.II.	Software (FORTRAN/COMPAS)	118

I. Introduction: Why Speckle Interferometry?

In 1976 The University of Arizona began a program under the Air Force Geophysics Laboratory (AFGL) with Laboratory Director's Fund support to develop image reconstruction techniques for large astronomical telescopes (Contract F19628-77-C-0063). Based on this program's success (AFGL-TR-78-0167), we began in 1977 this multi-year program to implement and improve the method known as speckle interferometry for studying telescopic images of objects of interest to the Air Force. In this final report on that project, we summarize methods we have developed for using speckle interferometry to recover high resolution optical information from images degraded by turbulence in the Earth's atmosphere.

Atmospheric turbulence reduces angular resolution for all large telescopes to about one arc-second, although theoretical limits for such instruments, as set by the telescope primary optics diameter, are up to fifty times smaller. For circular apertures, this limit is given by the well known Dawe's criterion:

$$\Delta\theta = \lambda/D \quad \text{nano radians (nrad)}$$

$$= 0.2063\ \lambda/D \ \text{milliseconds of arc (msa)}$$

where λ is the optical wavelength in nanometers and D the telescope diameter in meters. This formula predicts about 20 msa resolution for large telescopes like the Hale 5 meter, a factor of fifty better than the 1 arc second atmospheric "seeing" limit (about the size of a dime seen at 1 mile).

Although Michelson (1921) succeeded in using a form of interferometry to reach the theoretical resolution limit for observations of astronomical objects, it was not until Labeyrie's (1970) work that substantial further progress was made. Labeyrie pointed out that a short exposure photograph of a stellar image contans identifiable and extractable information on scales approaching the Dawe's limit given above. An example of short exposure star photos, at very large image scale, is given in Figure I.1. The overall size of these images is about 1000 msa. However, the small scale structure within each image has a scale very close to the 30 msa theoretical diffraction limit of the telescope used. The character of this small scale structure is noticably different for the three stars; a point source, a close binary, and a resolved supergiant star. These images, which have the characteristically "speckled" appearance produced by atmospheric turbulence, we call specklegrams. They are basically interference patterns. The process of extracting high resolution information from these interference patterns (sometimes called speckle images or speckle interferograms) is called speckle interferometry.

Atmospheric turbulence cells, regions over which small temperature differences and corresponding index of refraction changes can occur, break up the phase coherence of an incoming wavefront. These phase differences produce the interference patterns. To preserve high resolution information, speckle interferometry requires images on time scales short enough, typically 10 ms, to effectively freeze the interference pattern induced by turbulence in the Earth's atmosphere.

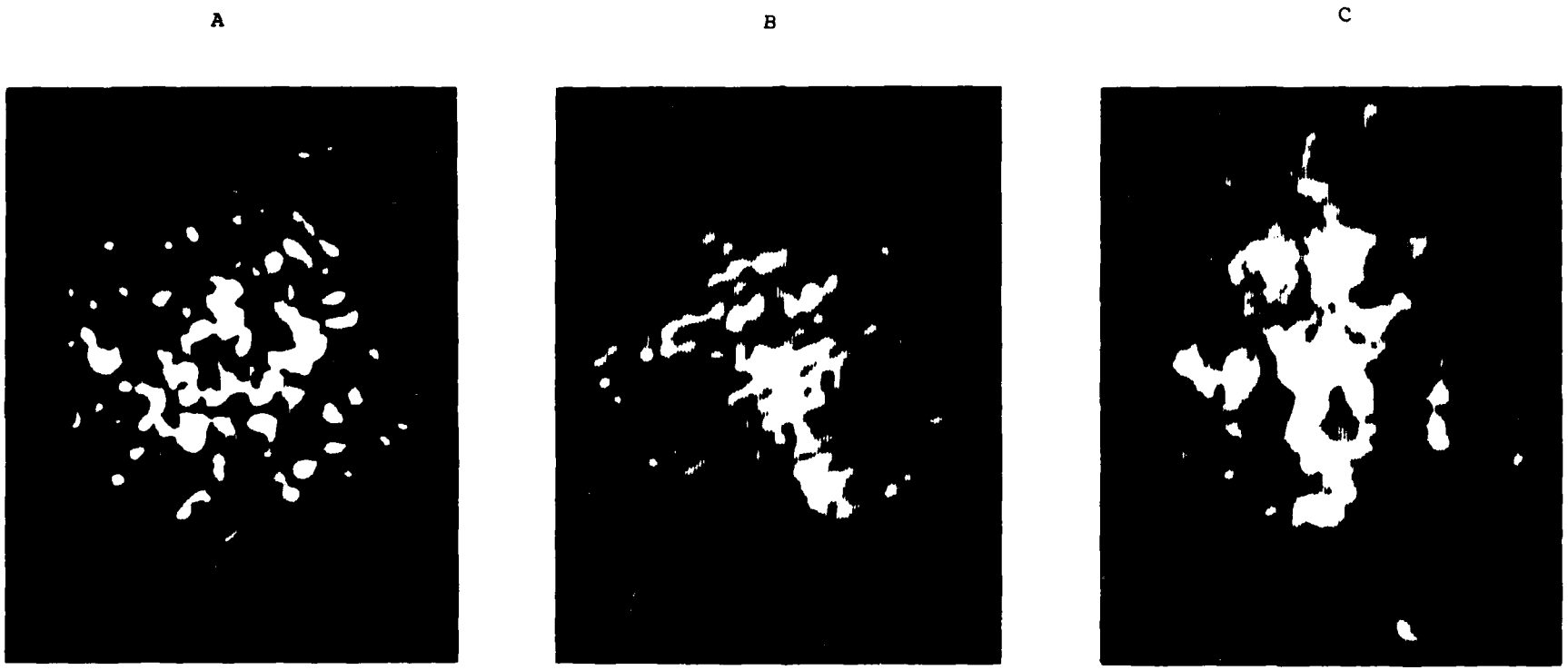

Figure I.1. Specklegrams taken with the Steward Observatory/AFGL intensified video speckle camera at the Kitt Peak National Observatory 4 meter reflecting telescope. Each covers about a 1 arcsecond patch in the 1.5 arc second square detector field. a) Gamma Orionis, an unresolved star; b) Capella, a binary star of nearly equal components separated about 42 milliseconds of arc; c) Betelguese, a resolved supergiant with an angular diameter of 60 milliseconds of arc.

A conventional long exposure photograph is a time average of signals, such as shown in Figure I.1, with rapidly varying wavefront errors. The long exposure image thus has a resolution set by the average scale of coherence (turbulence cell size)and (for large telescopes) not by the telescope aperture. The broken up wavefronts have significant phase variations on the scale of the atmospheric cell size (the "seeing" scale) rather than the full telescope aperture. This scale (called r_0 in the literature) is typically 10 cm, so that long exposure photos have resolutions appropriate to only a ten centimeter telescope, namely about one arc-second. However, in speckle images the turbulence is frozen by the short exposures and the ensemble of small 10 cm coherence phase errors acts as a form of multiple aperture interferometer and information on the full diffraction limited scale of the entire telescope is retained.

Speckle data were first reduced (Gezari et al. 1972) by optically producing the average power spectrum (Fourier amplitude) of many specklegrams acquired photographically. Such processing yielded diffraction limited size and shape information.

Classical power spectrum analysis does not, however, provide sufficient information to reconstruct a full diffraction limited image. Since 1970, an improved understanding of atmospherically induced image degradation has been reached and is reviewed by Labeyrie (1978), with special emphasis upon its astronomical applications. A tutorial prepared in conjuction with this project, entitled "THE AFGL IMAGE RECONSTRUCTION PROGRAM II.

Speckle Interferometry", published separately (Worden, Hege, Hubbard, and Strittmatter, 1981), summarizes mathematical details.

Two approaches, active optics and passive reconstruction based on extensions to speckle interferometry, have particular promise for complete image reconstruction. Active optics provide real time image compensation and reconstruction. However, they are costly and unacceptable for many Air Force uses, such as faint satellite imaging. This work has therefore concentrated on the development of passive, after-the-fact image reconstruction techniques based on speckle interferometry.

I.A. Status of Speckle Interferometry in 1977

When we began this project in 1977, the speckle technique suffered from two key problems which limited its usefulness: 1) Photographic recording systems limited speckle work to objects brighter than stellar magnitude +7, and 2) The data reconstruction techniques developed by Labeyrie and his collaborators provided not diffraction limited images but only diffraction limited Fourier amplitude information about the object being observed.

These early measurments produced angular sizes for bright stars and orbital data for binary stars. Although the object size and general shape are derivable from the Fourier amplitudes, the much more interesting diffraction limited image requires the Fourier phases as well. Existing telescopes such as the University of Arizona 2.3 meter, even with diffraction limited performance, provided only marginal angular resolution for high

orbit satellite studies or for many classes of interesting astronomical targets.

I.B. Summary of Objectives Proposed and Results Achieved.

We have divided our objectives for this project into five principle classes. We are pleased to report highly successful progress in meeting our objectives in every class. We briefly summarize the classes, objectives, and results:

1. Detectors. In 1977, photographic detectors were used to record speckle data. Photographic data are difficult to calibrate, have a low recording duty cycle (less than 1%), and are very cumbersome to reduce digitally for large numbers of frames. Under this contract we have developed a digital television detector system with the capability to identify individual photon events with a full duty cycle (100%) at 60 Hz. Using this system we have applied speckle techniques to objects fainter than +17 magnitude (10,000 times fainter than +7 magnitude, the limits in 1977).

2. Data Reduction. In 1977 data reduction methods relied on optical power analysis (Fourier amplitudes only) of speckle photos. This procedure produced size and shape information only, accurate to about 30% for objects of size comparable to the telescope diffraction limit. In 1977 actual images could not in general be obtained from speckle data. We have since developed data reduction and calibration methods that provide size and shape information accurate to better than 5% at the telescope diffraction limit. Moreover, we have produced actual diffraction limited images for several targets.

3. Scientific Targets. Largely as a result of inefficient data acquisition systems and poor calibration methods, speckle interferometry had produced only binary component and stellar diameter measurements for bright stars prior to 1977. By extending speckle techniques to accurate measurement of low surface brightness objects we have made several significant scientific observations: 1) we have measured diameters for over a dozen asteroids and possibly detected binary systems, 2) we have directly resolved and imaged the Pluto/Charon system, 3) we have resolved a multiple QSO (quasar) into at least five components, and 4) we have mapped and imaged asymmetries in the envelope around the supergiant star Alpha Orionis.

4. Military Targets. A principle objective of this program was to show the utility of speckle interferometry for studying Earth-orbital satellites. This task required developing pointing and tracking algorithms for satellite acquisition and tracking using conventional astronomical telescopes. We successfully accomplished this objective and produced the first optical resolution of a high orbit satellite, a Soviet Molniya.

5. Multiple Mirror Telescope Work. Even the largest single mirror telescopes do not provide sufficient resolution for studying synchronous satellites, or to make detailed maps of stellar surfaces. We therefore undertook a program to adapt and use the new Multiple Mirror Telescope (MMT), with an effective aperture of nearly 7 meters, for speckle interferometry. We have recently successfully combined separate MMT mirror beams to produce speckle results for stellar targets at the full 7 meter diffraction limit.

I.C. Areas for Future Development

We have identified four key areas for future development and exploitation of our results:

1. System improvements in hardware and software to provide near real-time results at the telescope.

2. Implementation of a dedicated speckle system for the MMT. We recommend an integrated system for the MMT with both infrared and optical interferometers. We are currently seeking support for this effort from other Air Force divisions.

3. We expect to continue using our existing system for military and scientific measurements. Our current system is particularly useful with telescopes like the KPNO 4 meter for faint object studies; for example, asteroids, galactic nuclei, QSOs, narrow band stellar surface observations, and intermediate altitude satellites.

4. Using the MMT as a test bed, we believe that new designs for extremely large ground and space based systems can be refined and optimized for imaging functions.

II. Speckle Interferometry at Steward Observatory

Speckle interferometric techniques have evolved from simple optical processing of photographic images to high-speed digital processing of quantum-limited video data. In this program to apply speckle interferometry to Earth orbiting satellites, and more generally to objects of astronomical interest, it was necessary to develop two areas: 1) Instrumentation to observe faint objects was required because most satellites of interest are much fainter than the brightest stars. 2) Data reduction methods suitable for general purpose speckle image analysis did not exist and had to be developed. We have now solved both of these problems. In this section we provide a brief description of the system and a demonstration of its use for studying an orbital satellite, in this case a Soviet Molniya communications satellite.

In speckle interferometry the power spectra, or equivalently the autocorrelations, of many specklegrams are averaged. These specklegrams are recorded at sufficiently high magnification that the spatial frequencies passed by the telescope aperture are well sampled. The exposure times must be short enough so that the atmospheric transfer function may be considered quasi-static through the duration of the exposure. Similarly, the bandpass must be sufficiently narrow that the speckegram may be considered quasi-coherent over the range of atmospherically induced phase shifts. Under these conditions, the resulting power spectra and autocorrelation functions can be made to yield diffraction

limited image intensity information. If, in addition, image phase information is accumulated from the same set of specklegrams, these image phases can be combined with the image power spectra to produce a speckle image reconstruction. This speckle image reconstruction provides a best estimate of the object intensity distribution at the resolution limit of the telescope - i.e. with atmospheric seeing effects removed.

Other important results of our work discussed briefly in this section include 1) preliminary success with speckle image reconstruction techniques applied to astronomical targets and 2) preliminary results in measuring objects at the diffraction limit of the Multiple Mirror Telescope. These successful techniques should also be applicable to satellite imaging.

II.A. The Speckle Camera

The Steward Observatory speckle camera (Hubbard, et al. 1979, Hege, et al. 1980a) is shown schematically in Figure II.1. From the top down, the components are

1) A microprocessor controlled zero-deviation antidispersion prism system.
2) A dichroic beam splitter to divert unused light into a wide-field viewing system, including an intensified vidicon system.
3) Interference filters to define the optical observing bandpass.
4) A microprocessor controlled Uniblitz shutter.
5) The telescope focal plane with provision for a knife-edge focus test and a calibration reticle.
6) Microscope objectives from 5X to 60X to set the final image sampling scale.

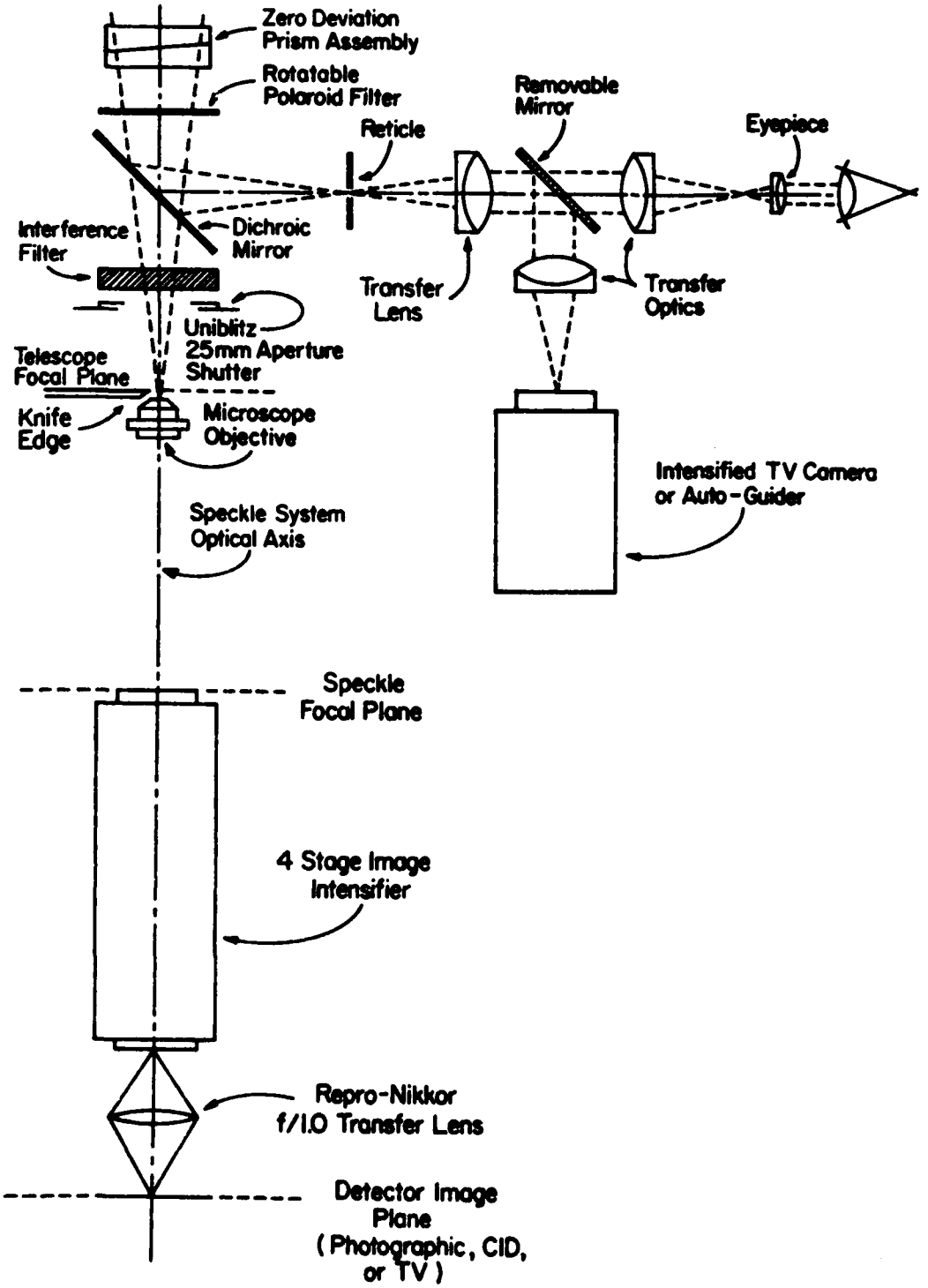

Figure II.1. The speckle camera. (See text)

7) Four stages of Varo electrostatic image intensifiers.

8) A Repro-Nikkor f/1 image transfer lens.

9) The final intensified speckle interferogram focal plane. In the present system a Plumbicon video camera is placed at this final focal plane.

II.B. The Digital Television System

The video data acquisition scheme is illustrated in Figure II.2. Video from the Plumbicon camera, consisting of 240 line video fields scanned at 60 Hz, is digitized 8 bits deep, 512 pixels per line, by a Grinnell GMR-27 digital television system. A Steward Observatory-specified arithmetic unit provides frame-by-frame video subtraction at video rates (Hege, et al. 1980a).

The primary video is transmitted to both the video memory and the + input of the subtractor. Before the previous value of a memory pixel is overwritten with the current value, that value is read back to the - input of the subtractor to produce the current video difference.

Logical processing permits implementation of two output data modes. In the analogue mode, image amplitudes are recorded for all pixel addresses. In the event mode, only lists of addresses of image amplitudes exceeding a given threshold are recorded. The amplitudes themselves are lost.

By operating the shutter synchronously with the video in analogue mode, the video difference produces specklegrams with the fixed pattern background subtracted. This allows shuttered exposures of 3 to 15 ms at up to 1/8 the 60 Hz video frame rate for bright objects. The event mode is used for objects

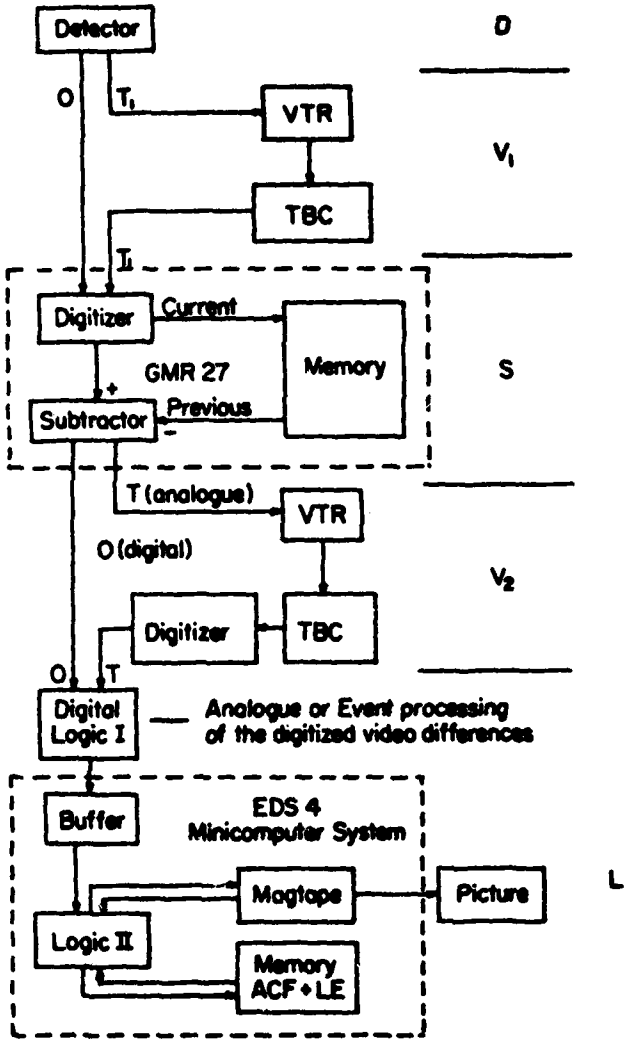

FIGURE II.2. The digital television system consists of the primary speckle detector (D), the video subtracting video digitizer (S), and the logical and computational subsystems (L) linked by video and analogue channels (V_1 and V_2). The Grinnell GMR-27 video analogue-to-digital conversion and digital video memory system, with especially designed video subtraction capability (S) is the primary video processing element of the system. The video difference may be output in digital format for on-line processing by Digital Logic I and/or as video analogue for later off-line processing, in which case it must be subsequently re-digitized. Video tape recording (VTR) provides a convenient, compact and cheap archival medium for the primary speckle interferometric data base.

sufficiently faint that individual photoelectron events do not overlap in successive frames. In the event mode the shutter is open continuously, the exposure time is set at 16.7 ms by the 60 Hz frame rate, and the duty-cycle is 100%.

Video tape recording of the primary video permits observation at sites without digital television systems. The video difference may be recorded for subsequent off-site processing if the on-site system cannot provide the required computational support necessary for on-line, real-time logging of digital data at video rates. Video tape records such as Sony U-matic 3/4 inch cassettes, which hold up to 60 minutes of observations, provide a reasonable primary archive for speckle interferometry data.

II.C. Speckle Data Reductions

We have developed data reduction software (Hege, et al., 1982a) to process both analogue mode and event mode data. These algorithms produce speckle autocorrelation functions (ACF), speckle power spectra (PS), and centered long exposure images (LE) for either analogue mode or event mode data. We have also experimented with two algorithms (Knox and Thompson, 1974 and Cocke, 1980) for image phase integration for analogue mode data. No image phase retrieval has yet been implemented for event mode data, although we are aware of an algorithm proposed by Mertz (1979) and a discrete-photon analysis of the Knox-Thompson procedure (Papaliolios, 1982).

For analogue mode data, the power spectrum is accumulated directly by Fast Fourier Transform techniques. For event mode

data, the ACF is accumulated as the histogram of differences in the event address lists. In both cases the LE is accumulated and used to produce a speckle image cross correlation function (XC) defined as the Fourier transform of the square modulus of the Fourier transform of the LE. This is used to produce an autocorrelation function and power spectrum corrected approximately for seeing.

The image phases produced by either method (Knox and Thompson, 1974 or Cocke, 1980) may be combined with the seeing-corrected power spectrum to produce an initial image estimate. A final image reconstruction is then achieved by Fienup iteration (Fienup 1978, 1979). Before use in the image reconstruction process, power spectra are treated by an iterative algorithm to remove any negative amplitudes induced by seeing and noise bias corrections. For faint objects for which no phases have been accumulated, the Fienup image reconstruction is initialized with random phases.

According to the basic theory of speckle interferometry (Labeyrie, 1970, 1978 and Dainty, 1975), a simple deconvolution using a similarly measured power spectrum for an unresolved source should produce the desired object power spectrum. If the speckle interferometric process can be characterized as a convolution of the object intensity distribution with a time dependent process representing the atmospheric "seeing"

$$i_t(x, y) = o(x, y) * p_t(x, y) \qquad \text{(II.1)}$$

then the time averaged PS of many speckle images

$$PS_o = \langle | I_t(u, v) |^2 \rangle_T = | O(u, v) |^2 \langle | P_t(u, v) |^2 \rangle_T \qquad (II.2)$$

can be deconvolved by a simple point-by-point division by a similarly processed observation of a point source PS to produce the desired object PS

$$O|(u, v)|^2 = PS_o / PS_\delta \qquad (II.3)$$

II.D Further Complications and Solutions

We have identified four categories of problems with this simple inverse filtering idea. 1) Temporal problems are mainly due to the time-dependent nature of seeing. The average process transfer function observed over one interval may differ from that observed over another interval. There is also a spatial analogue to this, as seeing may not be uniform over the sky. 2) Bias is an additive noise component, further complicated by details of the signal detection process. 3) The usual signal-to-noise problem of small numbers with large uncertainties becomes overwhelming when a quotient is involved. 4) Instrumental complications also arise. These refer to effects induced by peculiarities of the instrumentation itself.

II.D.1. Temporal Problems and Spatial Effects

Temporal problems can be controlled by good observing practice which requires that the calibration source be of similar brightness, in close proximity to the object, and that observations of the calibration source be interspersed with observations of the objects to assure similar conditions of seeing. We cannot over-emphasize the need for adequate care in making such calibrations.

II.D.2. Bias Effects

The simple deconvolution (II.3) has been found to be applicable only to the very brightest objects for which the noise due to the detection of individual photon events is negligible. When this effect is not negligible the measured power spectrum must be corrected for noise bias. The measured power spectrum

$$PS_O(M) = \{ < | FT(P_t) |^2 > PS_O + \bar{N} \} < | D_t(u, v) |^2 >_T \propto N^2 \quad (II.4)$$

where $\bar{N}$ is the mean number of photons per frame and the detection of $n >> 1$ photons with point-spread function $d_t(x, y)$ is assumed.

If photoelectrons were detected as delta-functions (unique pixel events), and if the probability of detecting an event were uniform over the surface of the detector (no vignetting), then the detector transfer function (DTF) = $| D(u, v) |^2$ would be unity. The point spread function for an ideal detector would at least be time and position invariant. These conditions are seriously violated by our system. Thus, in order to produce a deconvolved object power spectrum, it is necessary to correct both the measured power spectrum of the object, and that of the unresolved calibration star, for the mean shape of the detector transfer function, and then to subtract the resulting constant bias from both, before dividing. Thus,

$$| O(u, v) |^2 = \frac{PS_O(M)/D - \bar{N}_O}{PS_\delta(M)/D - \bar{N}_\delta} \quad (II.5)$$

We have investigated two methods for determining the detector transfer function: it can be directly measured in an independent calibration experiment, or it can be modelled. For a direct calibration, the detector is illuminated with uniform, low intensity light. The resultant data for these uncorrelated events is processed in the usual way. A model approach was suggested by an earlier analysis of our data by Fienup and Feldkamp (1980). We find that the photoelectron event intensity profile at the output of the image intensifier is approximated by a Gaussian. Therefore, the Fourier transform will also be approximately Gaussian. This model, unfortunately, ignores vignetting and other spatial non-uniformities of the detector. Another model approach uses a quadratic polynomial fit at radii corresponding to higher spatial frequencies to "recap" the autocorrelation function. By interpolating across the central spike, the noise bias is effectively removed. We have had some success with both the direct calibraion as well as the two modelling methods. Our analysis methods are, however, continualy being improved in this regard.

II.D.3. The Signal-to-noise Effects

We have not yet investigated the experimental details of the photon statistics problem. A simple argument illustrates that it is surely more complicated than the usual photometric Signal/Noise = $\sqrt{N}$. For faint objects not all photons carry speckle interferometric information. This is true because of the statistical, probabalistic nature of photon detection processes. If a speckle is defined as a place (typically the size of the

Airy function) where a partial wavefront, with a characteristic atmospherically induced phase shift, would come to a focus, there is no guarantee that a photon is actually detected in that place, only a probability of detection proportional to the stellar intensity. A single photon event in a single speckle carries no interpretable interferometric information. If the interferometer or the atmosphere has changed before the next photon is detected, the new interferometric information is uncorrelated with the old. Thus, at least two photons per speckle, so defined, are required to produce any useful interferometric information about a resolved object. At least one photon from each of two resolvable image features must arrive in a single speckle within the atmospheric correlation time.

For faint objects, this leads to the conclusion that useful information is accumulated as the fourth root of the number of photons detected per frame rather than the square root of N as for bright objects.

II.D.4. Instrumental Effects

Some of the additional instrumental effects are shown in Figure II. 3. The Sony VO-2800 video tape recorder "dropout" produces random noise along a line. The PS profile perpendicular to the line has excess energy at all frequencies. Large spikes are produced by a raster background periodicity in the output of the Microtime 1800 video time-base corrector. This instrumental noise analysis has been very useful in identifying possible instrumental improvements. For example, on-line systems will not have video tape recorder or time-base corrector artifacts.

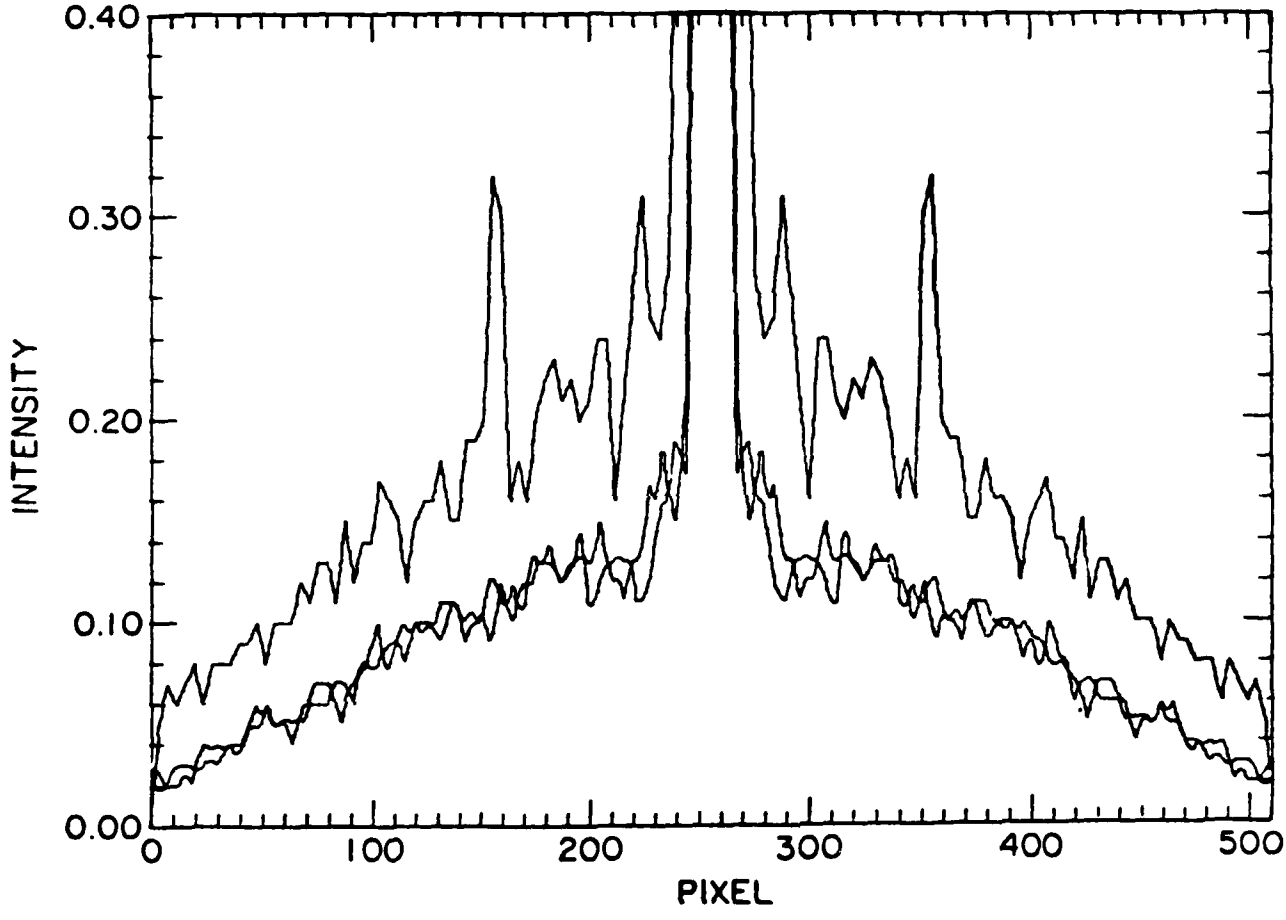

FIGURE II.3. Instrumental effects seen in a measured detector transfer function (DTF).

Ultimately, an image intensifier with better flat-field properties will be required. Fortunately, knowledge of the source of these artifacts suggests methods for correcting them. They are generally very localized in the power spectrum, and affect only a very narrow band of image frequencies.

Further details of the Steward Observatory/AFGL speckle camera, including preliminary image reconstruction results for Capella, Betelgeuse and Pluto/Charon, are found in Hege, et al.(1982a).

II.E. An Earth Satellite Observation

As a demonstration of our capabilities, we used our system to observe and measure a Soviet Molniya communications satellite. This object has a 12 hour orbit, during which time it moves from an altitude of about 5000 km to a synchronous distance of 40,000 km. With a size of about 5m, this object should be marginally resolvable, at these altitudes with telescopes like the University of Arizona 90 inch (2.3 meter) instrument. Despite its marginal suitability for study, we chose it since there are few objects large enough and at a high enough orbit so that relatively slow astronomical telescopes can both track and resolve them.

For our test, 15 minutes of data were obtained for the object on 7 July 1979 beginning at 02:50 UT. The mean range of this target during the observation period was 21,000 km. We also obtained a similar amount of data on a point source SAO 30753, an unresolved star, for comparison purposes. About 4×10^5 photons were detected for the target, an average of about 15 photons per

frame. We processed a sample of the data as described above to produce the power spectrum of both the target and the point source.

We did not try to recover the phase to produce an actual image of this object for two reasons. First, the object is only slightly larger than an unresolved object and it would not show much structure at our resolution. Second, the target spins once per second. The several minute observation period averages the spinning, so that only the pattern of the spinning solar panels would be visible, much as the spinning blades of a helicopter. Since the target is locked on the sun and we observed it at an angle, we expect to see only the oblong pattern of the spinning panels.

The autocorrelation function is very useful in studying the size and shape of an object. It follows that the autocorrelation of an oblong object would be oblong, and that of around object would fall to zero outside the diameter of the object. In this way, we can use the autocorrelation to measure the size and shape of a test target.

Since the target is only slightly larger than the telescope resolution limit, its autocorrelation is only slightly larger than the unresolved star. Nonetheless, the expected oblong shape is readily apparent. From the analysis we were able to derive a size of 4^{+2}_{-1} meters for the target, in excellent agreement with its actual size of 4.9 meters. The uncertainty in the result is set by our ability to remove the effects of the telescope itself, for which we use the observations of the point source star and

equation (II.5). This result has been published as an Air Force Technical Report (Worden, et al., 1979).

II.F. Speckle Image Reconstruction

We recognize that actual reconstructed images, rather than power spectra or autocorrelations, are essential if maximum information about the object in question is to be obtained. Based on our recent astronomical results, we are confident that recently developed methods will give us the phase information we need to completely recover images. We review our image reconstruction methods in this section.

An image i (x, y) is not uniquely determined by the image spectral amplitudes obtained from (II.5) or by Fourier transformation of those amplitudes. The full complex spectrum obtained by Fourier transformation, I (u, v) = FT (i), including phases as well as amplitudes, is required.

In the phase unwrapping method (Cocke, 1980), the phase angle ambiguity $\phi \pm 2\pi n$ $(n = 0, 1, 2, \ldots)$ is resolved by requiring the phase angles ϕ (u, v) to be as nearly continuous as possible as functions of the discrete wave-numbers (u, v). These phase angles are computed for each individual specklegram, are "unwrapped" by adding appropriate values of $2\pi n$ to get the required near-continuity, and are accumulated in a storage array. Thus, after the required number of specklegrams are processed, an average unwrapped Φ (u, v) is the result. Less ambiguity in n is obtained if the resolution in wave-number space (u, v) is improved by increasing the domain of the FT by padding out the speeklegrams with zeros. This increases somewhat the amount of

computer time and central memory required.

The Knox-Thompson (1974) method computes the phase factor ratios exp [i ϕ (u + 1, v) - i ϕ (u, v)] for each speckleg ram, at each value of (u, v), and accumulates them in a array, for averaging. The final result may be expressed, roughly as,

$$\exp[i\ \phi\ (u,v)]_{final} = \prod_{u'=1}^{u} < \exp[i\ \phi\ (u,v) - i\ \phi\ (u'-1,\ v)] > \qquad (II.6)$$

This method also benefits from increased resolution.

The image phases are then combined with the spatial amplitudes to form a reconstructed complex image spectrum. The seeing corrected PS usually contains non-physical negative amplitudes as well as non-zero amplitudes beyond the telescope aperture limit. We developed an iterative "cleaning" algorithm in which the PS and ACF pair are alternatively subjected to the appropriate non-negativity constraints, applied in both image space (ACF) and transform space (PS). Multiplication of the resultant cleaned PS by a suitable low-pass filter then suppresses the power beyond the aperture limit.

The reconstructed complex image spectrum, consisting of cleaned, filtered amplitudes and image phases, from either the Cocke or the Knox-Thompson method, is then further processed by the Fienup method (1978, 1979) to produce the final reconstructed image. This iterative method "retouches" the initial image estimate by using the cleaned, filtered, seeing corrected PS as a continuing constraint and further requiring that the image amplitudes produced be non-negative.

Analogue mode speckle interferograms for Capella, Betelgeuse and the unresolved star Gamma Orionis were obtained using the KPNO 4 meter telescope on 3 Feb 81. About 200 frames of data for each object, using a 10nm band-pass at 520nm, 15 ms exposure, and 14 msa/pixel detector image scale were processed by FT methods and equation (II.5) to produce seeing-corrected speckle power spectra.

We tested both phase-unwrapping and Knox-Thompson methods to produce images of the two resolved stars. In both cases the preliminary images were unrealistic in that some of the image amplitudes were negative. The Fienup retouching, however, cleaned these away and produced images in which the noise background had in both cases a rms value about 4 magnitudes fainter than the stelllar images.

There is only one element of significant phase information in a binary star image with unresolved components - the resolution of the 180° orientation ambiguity. Our result agrees with the orientation derived from the published orbit (McAlister, 1981). Our final result for Capella yields

Separation	$\rho = 42\ (\pm 1)$ msa
Position angle	$\theta = 151^{\circ}\ (\pm 2^{\circ})$
Relative intensity	$I_B / I_A = 0.63\ (\pm 0.05)$
Magnitude difference	$\delta m = 0.5\ (\pm 0.1)$

which compares favorably with Bagnuolo's analysis (Bagnuolo, 1982) by another method and with the previous analysis of photographic speckle data (Frost, et al. 1979).

The Betelgeuse image shows an asymmetry due largely to an

unresolved feature at position angle 208°. The excess brightness of this feature, compared to the brightness of neighboring image pixels is of order 25%. Since the mean diameter is about 60 msa and the measurement resolution is about 30 msa, the hot spot contributes an excess of order 25(±15)% in that unresolved image element or $\delta m = 0.08(\pm 0.05)$ to the integrated brightness of Betelgeuse. Our image analysis yields

Major dia.	63(±2) msa
Minor dia.	59(±2) msa
Position angle	208°(±5°)
δm (Feature)	0.08(±0.05)

The position angle is consistant with that obtained by Hayes (1982) using polarimetric methods. The images for both Betelgeuse and Capella are shown juxtaposed at the same image scale in Figure II.4.

The uncertainties in ρ, θ, and the diameters are principally limits in the precision of our image scale and camera orientation calibrations. The uncertainty in amplitude features are estimates based on dispersion in measures obtained directly from the power-spectrum fringe visibility functions and from the integrated amplitudes of the final reconstructed image components. The relative intensity determination may be subject to further systematic error due to image distortions produced by the electrostatic-focus image intensifiers in the present system.

We remind the reader that an uncertainty of 1 msa corresponds to an uncertainty of 0.2m in the measurement of the diameter of a resolved object in synchronous orbit at 40,000 km.

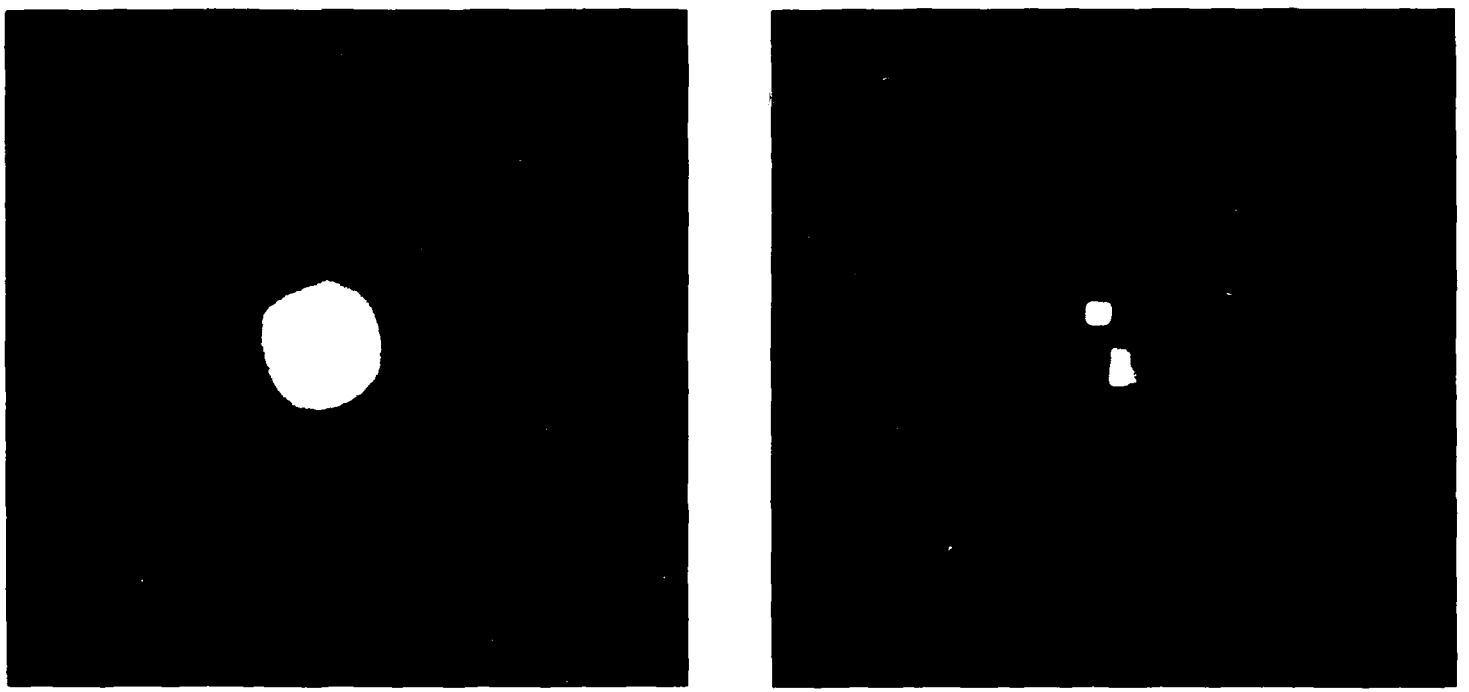

FIGURE II.4. Reconstructed images for Betelgeuse (left) and Capella (right). Phases by Cocke method. Retouched by Fienup method. Image scale is approximately 3 milliarcsecond/mm.

II.G. Speckle Interferometry With the Multiple Mirror Telescope (MMT)

Large gains in spatial resolution can be achieved by operating the 6.9m MMT in equal-pathlength configurations containing two or more telescopes. At present, pathlengths from radially opposite telescopes are equalized routinely at wavelengths of 0.5 um and 5.0 um. Measurements of the resulting Michelson fringes have characterized pathlength stability versus elevation angle, temperature, and perturbations of the optical elements. Effects of telescope pointing and tracking have also been measured. As a fully phased array, the MMT acts as an unfilled aperture responding in some degree to all of the spatial frequencies present in a filled 6.9m aperture. It also offers the potential to compensate for atmospherically induced image motion, thus enhancing the interference signal between individual mirrors. Instrumental designs have been developed to reconstruct a fully phased MMT pupil for joint scientific applications at optical and infrared wavelengths. Such designs must possess low infrared emissivity, must compensate for the polarization changes caused by non-normal reflections in the telescopes, and must eliminate the inclination of wavefronts produced by the standard beam-combining optics.

Figure II.5 presents a schematic diagram of the new prototype "optimized beam-combiner" which was used at the MMT in the standard focal mode to phase opposite-mirror pairs. This design, or any of several derivative designs, could be adapted to phase the entire telescope. The essential features are: 1) a

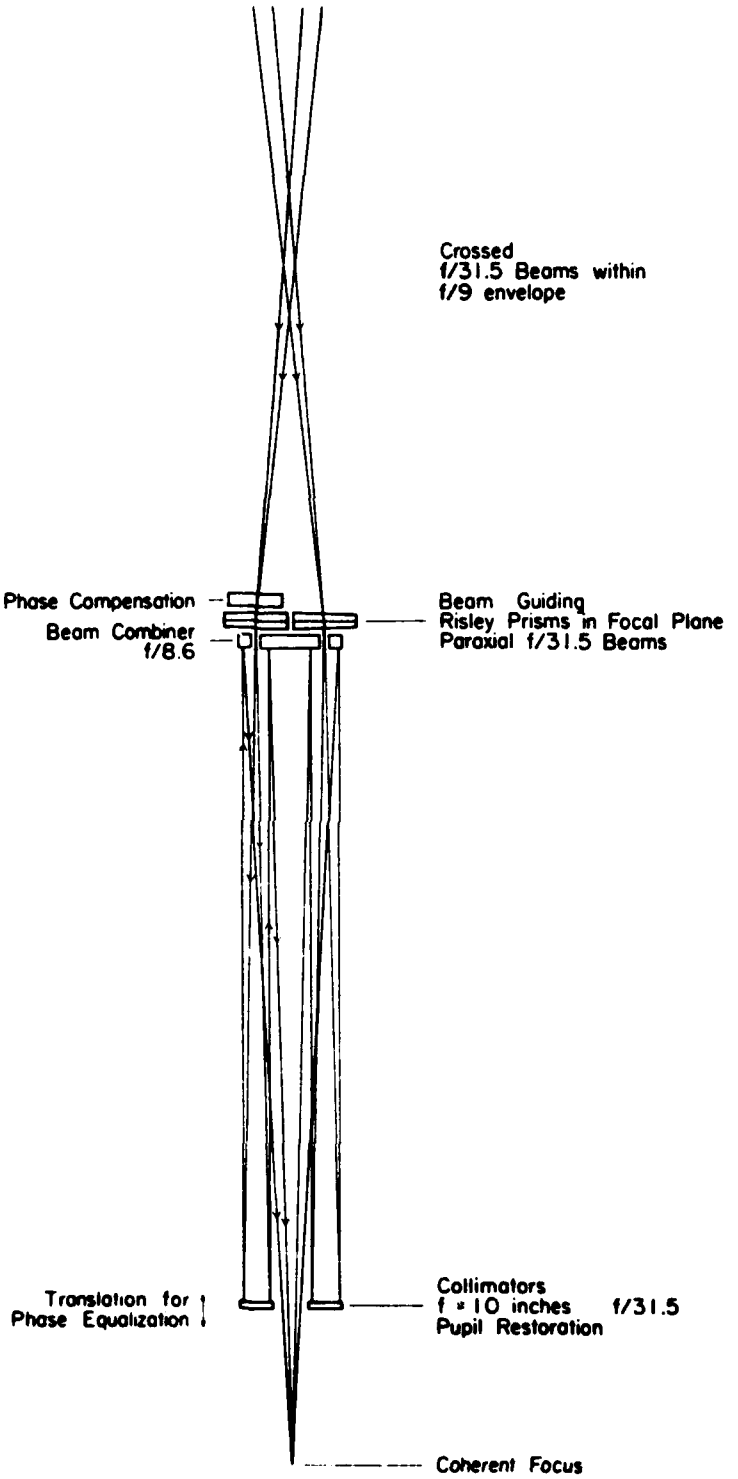

Figure II.5. Schematic diagram of coherent beam-combiner as described in text.

means to achieve coplanar wavefronts (a pair of prisms in the design shown), 2) a means to adjust pathlength (a micrometer controlled mirror in our prototype) and finally, 3) reimaging optics. The beam-combiner must be designed to recover the original MMT pupil geometry. In this prototype the two beams cross ahead of the instrument in order to avoid combining them inside-out in the final converging beam. Behind this optimized beam-combiner are the standard microscope lenses, optical filters and intensified speckle television camera used on other telescopes. The instrument rotator provides access to different mirror pairs.

Figure II.6 illustrates the resulting interference fringes obseved in a television frame (two 60Hz fields = 1/30 sec) after combining light from two 1.8 meter telescopes with center-to-center separation of 5 meters. The seeing envelop is somewhat less than 1 arcsec in diameter and consists of several speckles having angular diameters near the diffraction limit of the individual telescopes (about 0.1 arc second). As expected from the geometry of the MMT, approximately three fringes are observed in each instance where speckles from opposite telescopes overlap. No degradation in fringe visibility was observed as the mount was mispointed over a 5 arcsec range demonstrating that a coherent field has been achieved as desired; larger fields could not be explored due to the finite resolution of the speckle camera and the small fringe widths. In addition, a double star, Alpha Geminorum (2.3 arcsec separation), was observed with both components displaying fringes simultaneously (Figure II.7). This

FIGURE II.6. Interference fringes observed on point source in a single television frame (1/30 sec). This picture is 0.6 arcsec on a side. Nearly vertical fringes (15 msa) are observed where speckles from the two telescopes overlap. More finely spaced horizontal lines are TV scan lines.

test confirmed the expected performance of the beam combiner design.

The coherent beam-combiner cannot distinguish between image motions caused by mount tracking errors or by telescope flexures (e.g., secondary mirror tilts). The former generate pathlength errors across the 5 meter mirror-center to mirror-center baseline whereas the latter do not. The coherent beam-combiner makes the MMT behave as a single telescope yielding a phased field: ..e. it automatically corrects pathlength differences caused by tracking errors or by differing positions in the focal plane. However, it also inserts pathlength corrections for flexure related image motions when none are required, thereby destroying coherence. Consequently, in any phasing concept for the MMT, it is desirable to minimize tilting motions of the secondaries. This requires both improved structural stability of the optics support structure (efforts to achieve this condition are already in progress by the Multiple Mirror Telescope Observatory). The new Telescope Coalignment System (TCS) (now nearing completion) must not use the secondaries to correct for mount tracking errors. It is desirable to improve mount tracking to maintain an image well within the approximately 1 arcsec detectoraperture. The recently adopted goal of < 0.2 arcsec rms tracking error meets our requirements. For accurate calibration of the interferometer MTF, the mount should offset to < 0.2 arcsec rms precision over at least a 3^{o} range on the sky.

For interferometric work it is essential to minimize both mount pointing errors and flexure-related tilts of the telescope

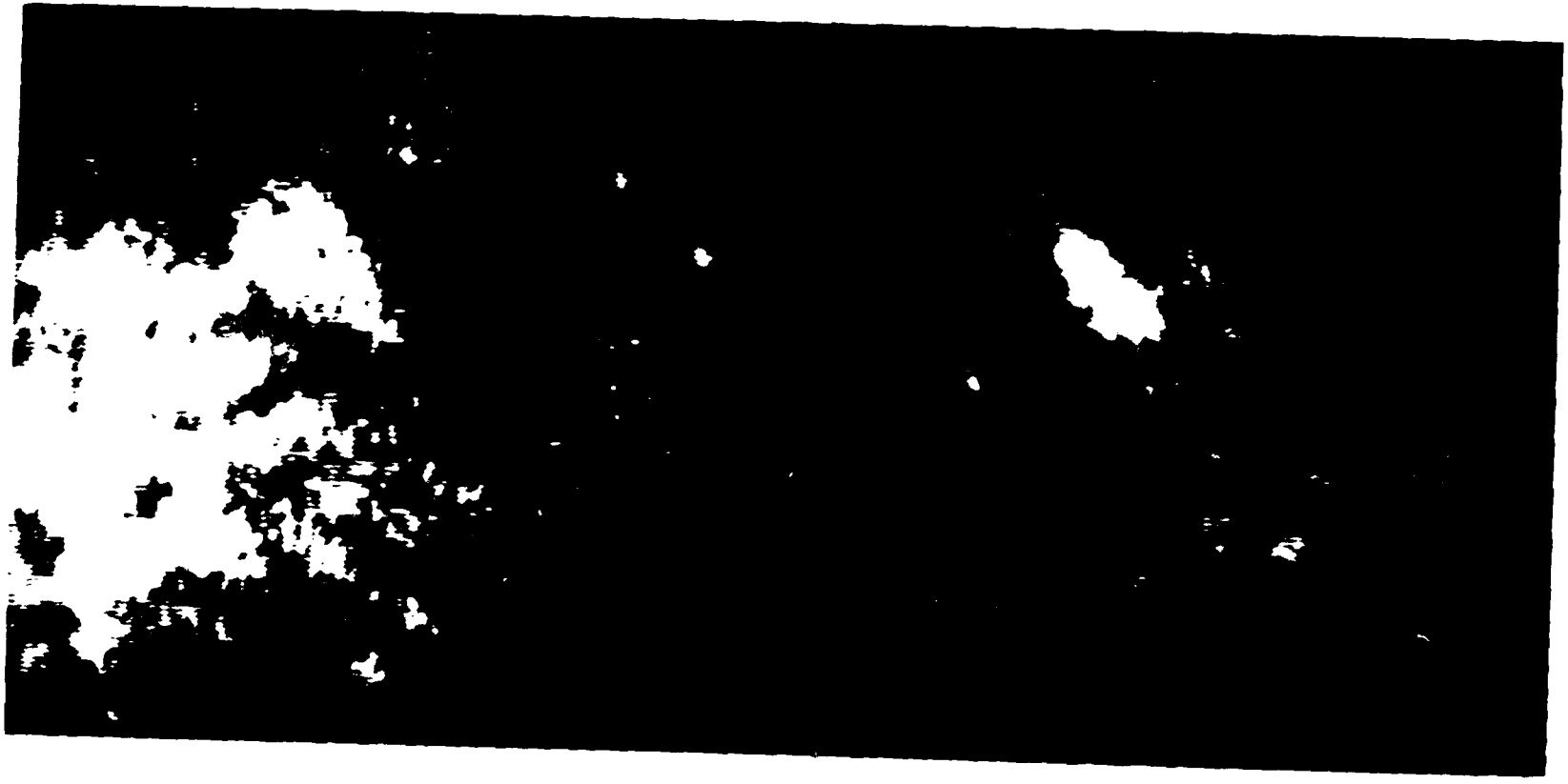

FIGURE II.7. Interference fringes observed in both components of α Gem. The interferometer is slightly de-tuned so that the fringes are seen only in the right-hand half of each speckle cloud. Tthe fringe contrast appears degraded due to the limited resolution of the video detector system. (See section V.C.)

optics. It is also necessary to distinguish between these two effects when correcting for image motions. If mount tracking were "perfect", corrections for secondary tilts could be achieved unambiguously. If there were "no" tilt errors, mount pointing errors would become only a problem of inconvenience and could be guided out as at a normal telescope. A combination of these imperfections is more difficult to handle and work is currently underway, in conjunction with the MMT Observatory,

1) to reduce pointing/tracking errors;
2) to reduce flexure/hysterisis in the optics support structure/mirror supports, etc.;
3) to develope TCS software which recognizes that pointing errors must, as far as possible, be corrected by the mount and not by the secondaries.

In addition, an algorithm has been developed for on-line correction of path-length errors which, when implemented, should solve any residual problems.

During our observations, several scientific experiments were performed. Figure II.8 illustrates a measurement of the angular diameter of Alpha Taurii (Aldebaran) at 750 nm. Part a) shows the measured visibility function of Alpha Taurii which was slightly over-resolved with the 15 msa resolution available here. The data are fit well by a uniform, circular disk model having an angular diameter of 23.6 msa in excellent agreement with the values of 23.1 and 22.2 milliarcsec obtained recently from lunar occultations (Radick and Africano, 1981). Part b) shows the power spectrum of the comparison source, Beta Taurii, observed

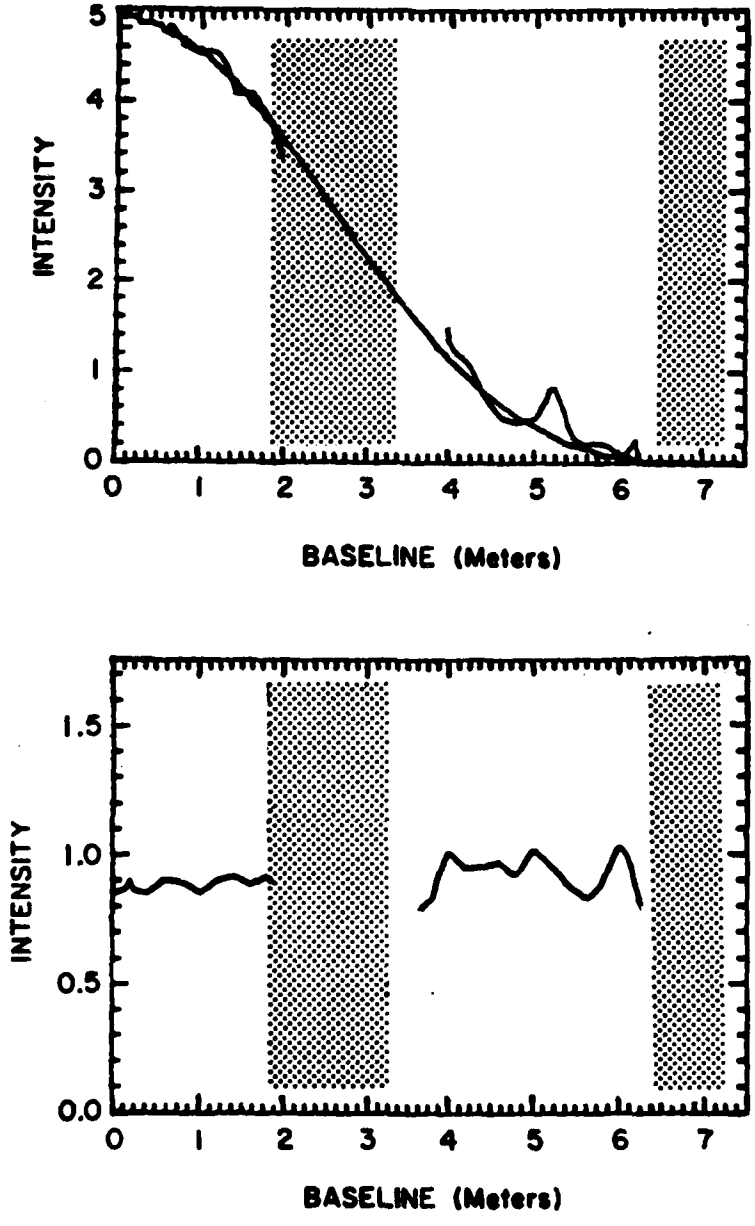

FIGURE II.8. a) power spectrum of (α Tau/< β Tau>) versus spatial frequency. Beta Tau was observed before and after α Tau and the averaged power spectrum was used to normalize α Tau. Solid line is the expected response from a uniform circular disk of 0.022 arcsec angular diameter. Spatial frequencies corresponding to baselines from 1.8 to 3.3 m and > 6.9 m are not omitted in the figure. b) power spectrum of first β Tau measurement divided by the averaged β Tau measurement. Perfect conditions and unchanging path-equalization would yield a horizontal line at 1.0.

before and after Alpha Taurii; the repeatability is excellent and the response shows the expected components both at low spatial frequencies from the individual 1.8 meter telescopes and also at high frequencies from the combination. Observations were also made of Capella. The binary nature of this object was clearly identifiable through the characteristic fringe pattern in the power spectrum. Again, the measured position angle and separation agreed well with the published orbit. In fact, this object is sufficiently resolved for the second fringe minimum to appear in the power spectrum -- at the 4-meter telescope only the first fringe minimum is detectable. This clearly demonstrates the expected improvement in resolution provided by the larger optical baseline.

Additional measurements were made of Betelgeuse, which should be well over-resolved at this telescope, to study limb-darkening effects; these have yet to be reduced.

III. Atmospheric Seeing and Speckle Interferometry

III.A. Effects of Dome Seeing

One of us (Woolf, 1979) has undertaken an analysis of the degradation of seeing caused by thermal effects in the immediate environment of the telescope. Empirical relations between seeing and thermal dissipation in the dome could be understood quite well in terms of mixing length theory of thermal convection. Methods for reducing thermally induced seeing, including basic design parameters for building and dome, were analysed.

III.B. High Resolution Imaging from the Ground

A series of studies and experiments have been carriedout to determine i) how well the theory of seeing as developed by Fried and others matches the observational data and ii) what influence this should have on telescope location, design, adaptive optics etc. The basic conclusions are as follows:

a) The theory of seeing provides a good model for seeing arising in the upper atmosphere.

b) Observations indicate that the seeing arises from two princple sources, namely, from the upper atmosphere and from the immediate proximity of the telescope - that is, in the dome itself or in a thin boundary layer whose properties depend very much on local geography.

c) There is little variation in the upper atmospheric properties among established observing sites.

d) Local seeing problems can to a considerable extent be controlled or avoided if sufficient attention is paid to site selection and construction technique.

e) Local seeing conditions tend to be more difficult to control on sites that are dry and have large diurnal temperature variations. Both dryness and good seeing are essential for IR work so that it is essential to address both problems simultaneously.

f) Local seeing tends to control image size at most sites and times; it is not normally associated with significant image motion owing to a small outer scale of turbulence.

g) For upper atmospheric seeing image motion and image size are well correlated. At typical observatory sites the mean image wander is $\sim$ 0.2 arcsec and image size is $\sim$ 0.5 arcsecs at visible wavelengths for an $\sim$ 2 m telescope. The image size decreases significantly with increasing wavelength whereas the image wander is essentially independent of wavelength. The ratio of image wander to image size decreases as the aperture increases.

h) Significant improvements in "long exposure" image size can be achieved by image centroiding for medium apertures and by active optics for larger telescopes. The gains are especially significant at infra-red wavelengths where the parameter r_o (the separation in the pupil associated with an rms phase difference of one radian) is large ($\sim$ 2 meters). At optical wavelengths the value of r_o is sufficiently small that active optics can only provide significant gains in rather special circumstances.

A review entitled "High Resolution Imaging from the Ground" has been prepared by Dr. Woolf and is to appear in Annual Reviews of Astronomy and Astrophysics.

III.C. Influence of Telescope and Atmospheric Distortions on Speckle Interferometry

As part of our development of speckle techniques at the telescope we have investigated a number of parameters which could affect speckle sensitivity. These included telescope focus, spectral bandwidth and exposure time. The absolute effects are all dependent on the atmospheric conditions and are thus highly time dependent. For this reason, data is still being accumulated. Nonetheless, some general trends are clearly discernible. Our principal conclusions are as follows:

a) The speckle transfer function is not strongly affected by telescope focus - or other abberations - as long as the amount of defocus is less than the size of the seeing disk. The result confirms earlier theoretical and observational work by other groups. As the aberrations become comparable with the seeing scale, transfer efficiency at the higher spatial frequencies is degraded.

b) Our results indicate, as expected, a degradation of high spatial frequency response as the relative bandwidth of observation $(\Delta\lambda/\lambda)$ increases above a critical value given approximately by $(\Delta\lambda/\lambda) \approx d/s$ where d is the telescope diffraction limit and s is the seeing disk size. The fall off is, however, relatively slow. This conclusion is both gratifying and somewhat puzzling; it is tentatively ascribed to a relatively high information content in so-called zeroth order speckles. The

conclusion is further demonstrated by our experience in observing the faint QSO PG1115+08 (cf. section IV.A). One set of observations was made without any filter at all, ($\Delta\lambda / \lambda \approx 1/3$). The resolution was degraded from 0.07 arcsecs to only $\sim$ 0.15 arcsecs.

c) Experiments on exposure time indicated a fairly strong dependence of speckle sensitivity on this parameter. The SC/AFGL speckle camera is limited in its normal operation to frame times exceeding 16 ms but shorter exposures can be obtained through use of a shutter and through sacrifice of duty cycle efficiency. Our results are very much dependent on atmospheric conditions. The transfer efficiency at higher spatial frequencies declines rapidly relative to that at lower frequencies if the exposure time exceeds the characteristic variation time of the atmosphere. For shorter exposures the relative frequency response is maintained but the absolute sensitivity is reduced as the exposure time is decreased. These results are in qualitative agreement with theoretical analysis by Dainty (1974).

III.C.1. Image Wander

The largest-scale effect of the atmospheric disturbance of the incoming wavefront is to cause, on the average, a tilt across the segment sampled by the full telescope aperture. This produces a shift in the mean position at which the image is detected in the telescope focal plane. This image wander has no effect on ordinary single-aperture speckle interferometry as long as the field is large enough so that the image does not wander outside the observing field. The effect is important for

multiple-telescope interferometry, however, where the light from each of the component beams must be accurately superimposed. It is also important at image scales such that the field size is comparable to the scale of the image wander. A related question is: Can the image quality be significantly improved by simply correcting these first-order tilt errors?

We have measured this component of the image motion on various occasion at several telescopes, Table III.I. Two effects are seen

Table III.I Image Wander

Telescope	Bandpass	Seeing*	Image Wander (Peak-Peak)
2.3m	550/30 nm	1".5	0".6
1.8m	700/100	0.5	0.6
4 m	550/10	0.5	0.4

*FWHM after image wander effects have been removed.

Qualitatively, the image wander appears to be more nearly independent of seeing than one might have expected, and the principle effect appears to be an inverse dependence upon aperture size. Two qualitative kinds of seeing are identified, one in which there are rapid variations in phase at small scale across the aperture with correlation time comparable to or smaller than our detector exposure times and larger scale variations with longer correlation times. These are qualitative definitions of "poor seeing" and "good seeing", respectively.

Under poor seeing conditions the image wander component makes a negligible contribution to the over-all image size, while for good seeing the two components are comparable.

Figure III.1 shows the result of direct imaging of a $m_V = 15.7$ QSO, PG1115+080 produced by rapid guiding - a technique by which the image wander is removed exposure-by-exposure. Figure III.2 shows the corresponding guiding corrections. The low-frequency, approximately harmonic variations are due to periodic errors in the telescope position; the high-frequency variations of lower amplitude superimposed upon these low-frequency variaions are a measure of the atmospherically induced image wander. The individual frame exposure time for Figures III.1 and III.2 was 0.5 sec. The presence of structure at a scale of tenths of an arcsecond is detected in the brighter component while the two fainter components are unresolved at 0.6 arcseconds FWHM. Speckle interferometry on the following night under similar seeing conditions clearly resolved the brighter component into two components of similar brightness separated by 0.54 arcseconds at a resolution of about 0.13 arcseconds (See section IV.A.).

Figure III.3 shows a direct image of the Pluto/Charon system produced by rapid-guiding at 30Hz. In this image of 0.3 FWHM, the faint satellite is marginally detected at the position shown by the arrow. Using this same data set, the separation of Pluto/Charon was measured to be 0.34 (well resolved) by speckle interferometry. (See section IV.B.)

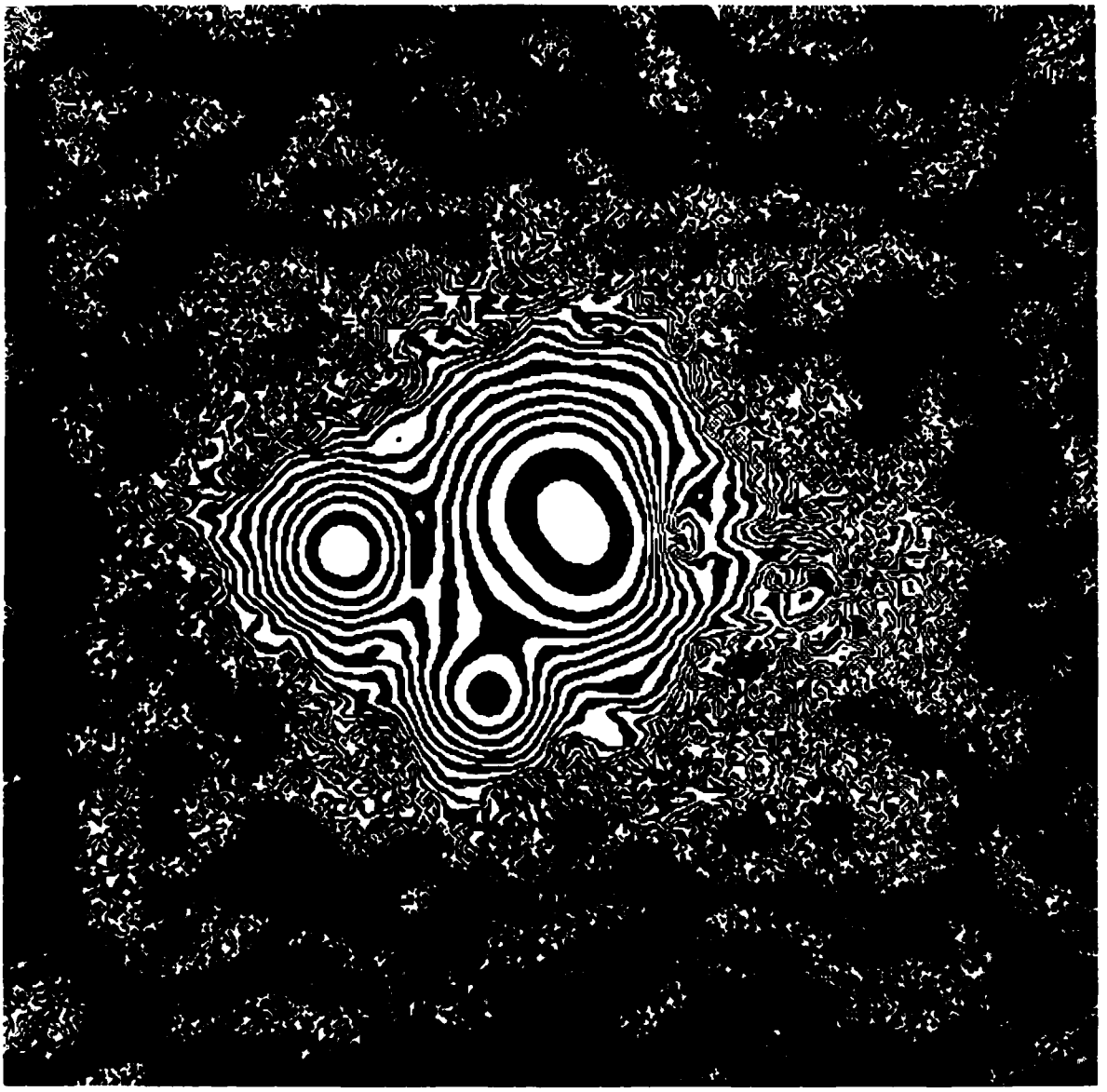

Figure III.1. PG 1115+080 direct image. Superb seeing at the MMT site was exploited by post-detection rapid guiding to produce this image, uncorrected for seeing, with PSF = Ø.6 arc seconds FWHM.

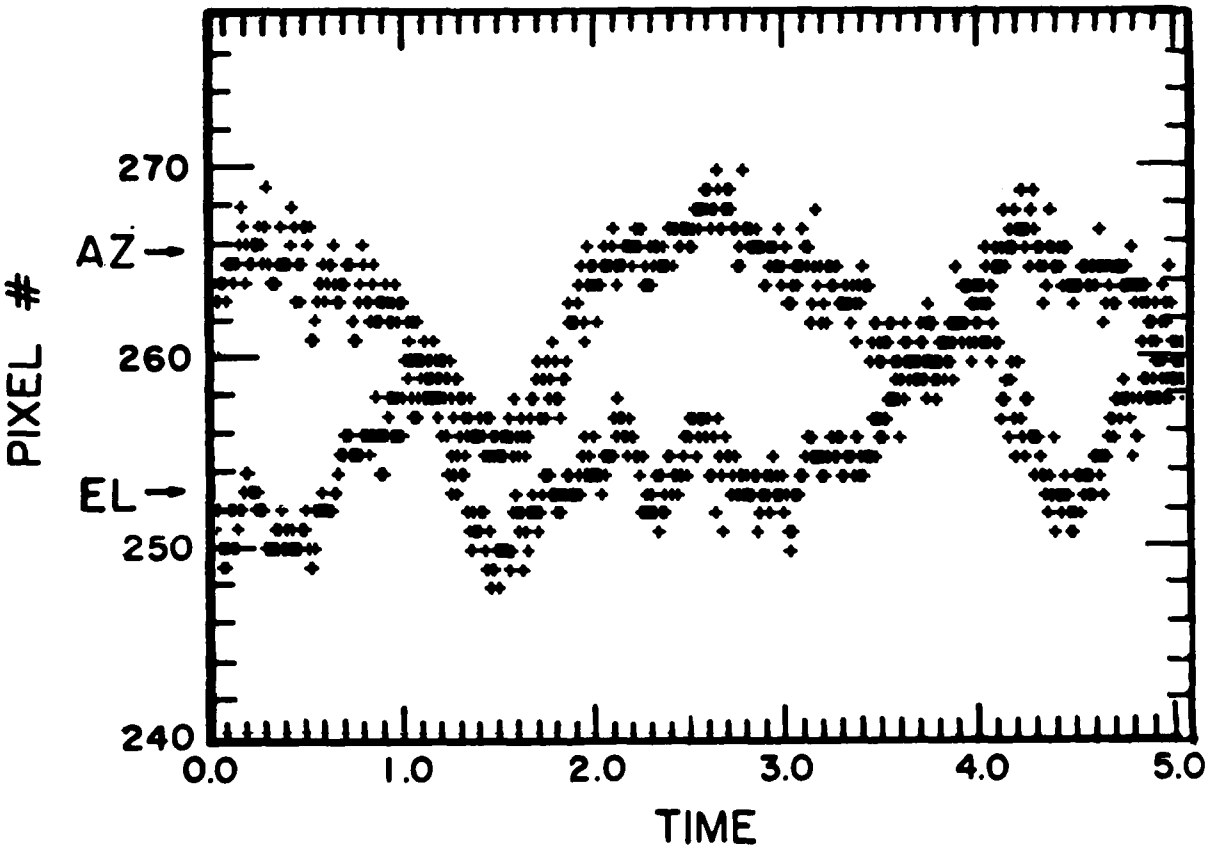

Figure III.2. Tracking record for observation in good seeing at MMT. The large-amplitude (about 1 arc second) nearly periodic variations are due to residual encoder errors affecting the telescope pointing. The small-amplitude (about 0.3 arc second) high-frequency variations are due to seeing. Both of these effects were removed by post-processing rapid-guiding in order to produce the result shown in Figure III.1.

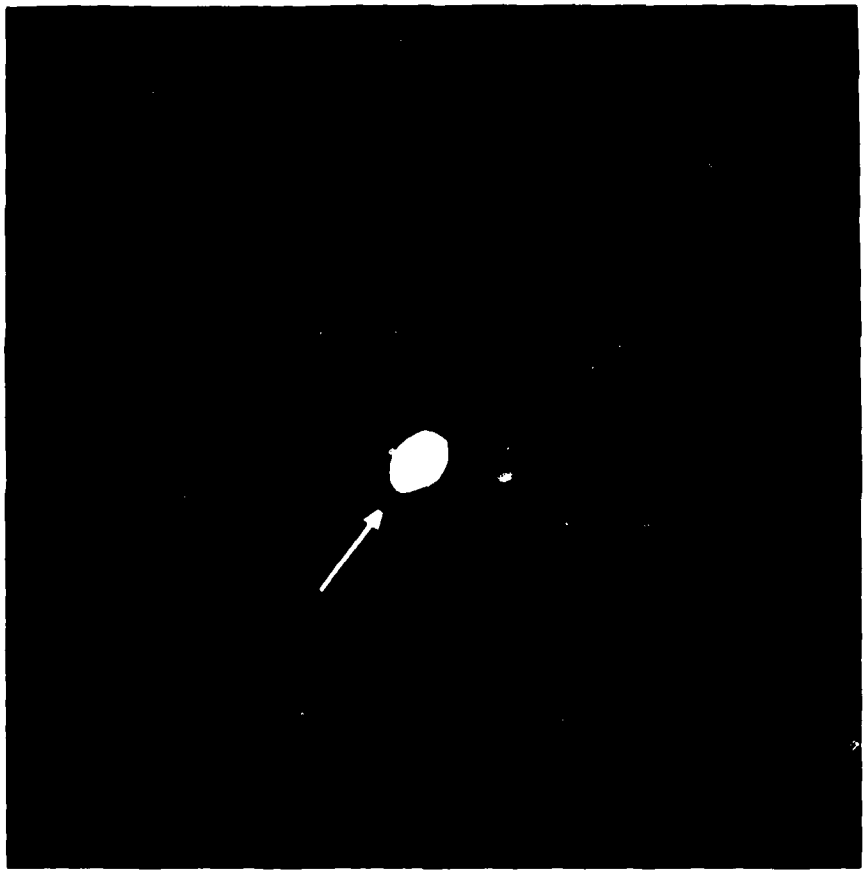

Figure III.3. Pluto, direct image. This exposure, rapid-guided by superimposing re-centered video frames at 60 Hz, produced an image of Pluto and its satellite with PSF = 0.3 arc seconds. The satellite was 0.34 arc seconds from the center of Pluto, at the position angle shown by the arrow. (See Hege, et al. 1982b).

Careful attention to the consequences of image wander is important in achieving the ultimate interferometric contrast in a multiple telescope interferometer. A typical two-telescope specklegram is shown as Figure II.6 in section II.G. Fringes are seen only in the parts of the image where light from telescopes is superimposed. One can define an interferometric contrast which varies from 0 (no overlap of images) to 1 (perfect superimposition of identical speckle images). Figure III.4 shows the MTF measured by summing the Fourier amplitudes of a set of such specklegrams. The dotted curve shows a fit characterized by interferometric contrast 0.16. A qualitative argument shows that this is both typical for such seeing conditions without rapid guiding and subject to severe deterioration if the individual telescope speckle images are not well-centered. For good seeing (1 arc second or better), as in the case of this experiment, relatively few speckles contain a significant fraction of the total beam intensity at any instant. For a 1.8 meter telescope, these speckles are about 0".1 in extent and are distributed in the 1".0 extent of the seeing distribution with largely uncorrelated phases as the two telescopes sample independent air masses. Since there are $O(10^2)$ single mirror speckle resolution elements in the seeing distribution, and typically O(10) principle speckles, only about 10% of the seeing distribution is filled at any instant. Thus the observed 16% interferometric contrast suggests better than random overlap. This is not surprising since the distribution of speckles within the seeing distribution is not random but concentrates towards the center, and the

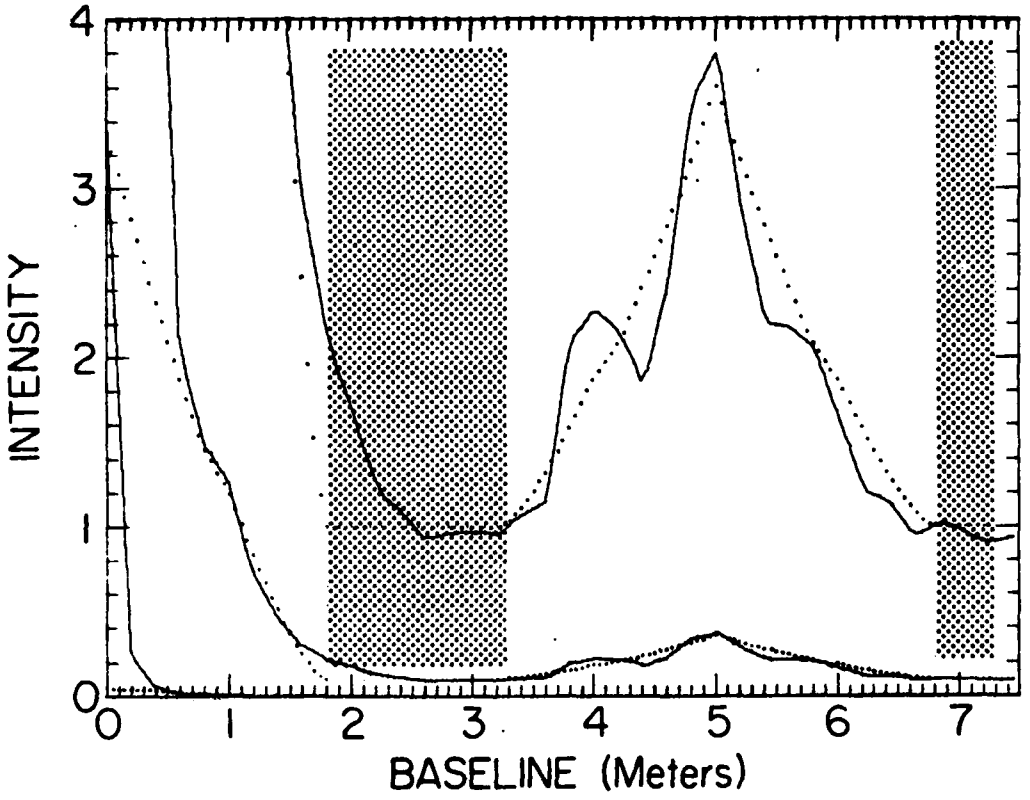

Figure III.4 MTF for two-beam MMT interferometer. This is an intensity profile through the average power spectrum of many specklegrams such as Figure II.6. The cut is taken in the direction along the line connecting opposite MMT mirrors (perpendicular to the fringes in Figure II.6).

centers of the seeing distributions were approximately superimposed but without rapid guiding.

If the interferometric contrast as measured by the amplitude of the MTF is proportional to the probability of overlap of speckles from different apertures, then the 16% amplitude implies a 40% probability that a given point in the specklegram contains light from both telescopes.

Let the probability of finding a speckle at point x from a particular telescope be given (approximately) by

$$\rho(x) = \rho_0(\sigma)e^{-x^2/\sigma^2} \tag{III.1}$$

where σ is a measure of the seeing and $\rho_0(\sigma)$ represents the probability that this distribution is filled, as described above, and

$$\rho(x, x_o) = \rho_0(\sigma)e^{-(x-x_o)^2/\sigma^2} \tag{III.2}$$

be the probability of finding a speckle at point x from a second telescope whose image has shifted by x_o (either due to image wander of to poor telescope coalignment). We will assume identical telescopes and similar seeing for both so that $p_0(\sigma) = p_o$ for both. Then the probability of overlap of speckles from both telescopes at point x, given by the product $p^2 = \rho(x) \cdot \rho(x, x_o)$ has a new local maximum ($dp^2/dx = 0$) at $x = 1/2\ x_o$ given by

$$\rho^2_{max} = \rho_o^2\ e^{-x^2/2\sigma^2} \tag{III.3}$$

Table III.II shows this combined probability maximum as well as that for speckles from 6 telescopes (as in the MMT).

Table III.II.

Predicted Effect of Seeing on Interferometric Contrast

x_o	P_{max}	P_{max}
1/4 σ	0.97 ρ_o	0.91 ρ_o
1/2	0.88	0.68
3/4	0.75	0.42
1	0.61	0.23
5/4	0.46	0.10

We conclude that rapid guiding, on time-scales comparable to that used to produce the images shown in Figures III.1 and III.3 can produce a substantial improvement in the speckle interferometric contrast.

Since sub-aperture rapid-guiding phase corrections can reduce the area over which the light is distributed in the focal plane, compared to the distribution produced by an un-corrected single aperture of equivalent dimensions, the faint object performance of such a system is improved. The effective seeing is that of the individual telescopes but the light gathering capability is that of the larger aperture. Initial tests of the MMT focal-plane, digital-television Telescope Coalignment System (TCS) show that it is expected to keep all six beams superimposed at about 0".1 rms.

III.C.2. Effect of Telescope Focus

The dependence of the MTF on telescope focus has been measured. The average Fourier amplitudes (MTF) for a set of specklegrams for each of a series of focus settings using the Steward 2.3 meter telescope was obtained. The results are presented two ways in Figures III.5a and III.5b.

In Figure III.5a the MTF with largest high-frequency response was taken to define "best focus". Each MTF was divided in turn by that best focus MTF. The systematic high-frequency fall-off with focus degradation is easily seen. In Figure III.5b the autocorrelation functions for a resolved binary star are shown displaying corresponding degradation of the high-frequency image response. Three units corresponds to a shift in focus of 1mm at the 2.3 meter telescope at the f/9 focus where the image scale is 10"/mm. Thus we conclude that a significant loss of contrast occurs when the focal "circle of confusion" approaches the instantaneous seeing scale. That is, good telescope focus criteria for conventional high-quality direct imaging applications may be inadequate for speckle interferometric applications.

This focus dependence of interferometric contrast led us to add a knife edge focus test capability to our speckle camera. After some experience with this system we became proficient in visually judging the quality of focus by inspecting the hardness of the speckles in the central regions of the seeing distribution. Using this method we can usually set the telescope focus to about 1 unit precision (0.3 mm) in good seeing.

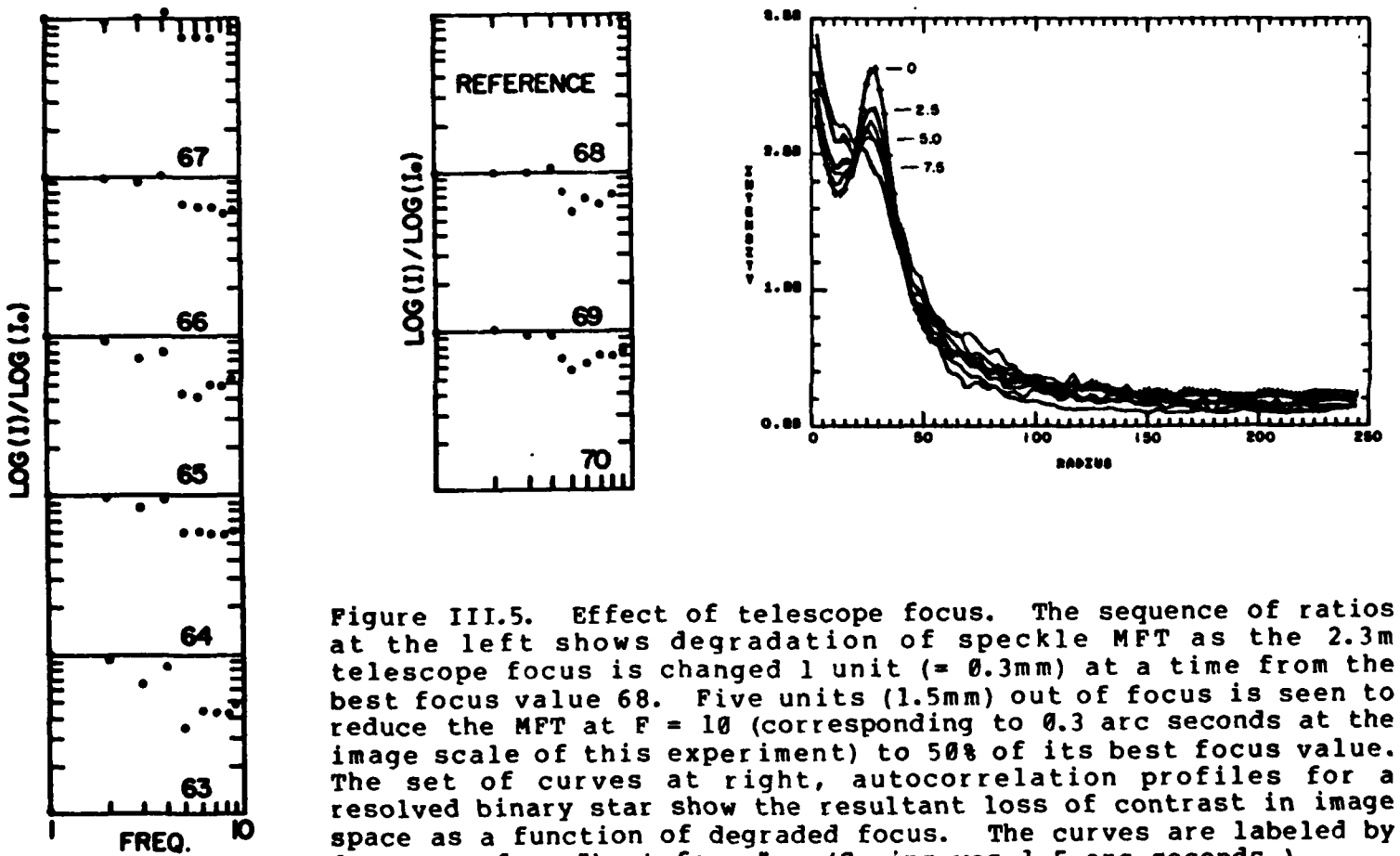

Figure III.5. Effect of telescope focus. The sequence of ratios at the left shows degradation of speckle MFT as the 2.3m telescope focus is changed 1 unit (= 0.3mm) at a time from the best focus value 68. Five units (1.5mm) out of focus is seen to reduce the MFT at F = 10 (corresponding to 0.3 arc seconds at the image scale of this experiment) to 50% of its best focus value. The set of curves at right, autocorrelation profiles for a resolved binary star show the resultant loss of contrast in image space as a function of degraded focus. The curves are labeled by departure from "best focus". (Seeing was 1.5 arc seconds.)

Another focus effect may be significant for observing objects in the near-field with large astronomical telescopes. At 10^4 Km the focal-plane of the 2.3 meter f/9 telescope has shifted 0.043 mm and at 10^3 Km it is 0.43 mm behind the focal plane for an object at infinity. Some adjustment of telescope focus may be required for optimum observation of such objects.

III.C.3. Effect of Observing Bandpass

Preliminary evidence suggests that the optimum bandpass for speckle interferometry is highly seeing dependent. The details of this dependence have not been fully explored, but experience has shown that for good seeing larger bandpasses can be utilitized. Figure III. 6 shows the results of observations of the binary star ADS 9744 with the 2.3 meter telescope on a night when the seeing was good to average (1.5 to 2.0 arcseconds). Considerable loss of contrast is seen in this observation at 550 nm when a 30 nm bandpass is compared to a 100 A bandpass.

We have, on the other hand, successfully observed at 600 nm with much wider bandpass 60 nm (See IV.B.) and 200 nm (See IV.A.), under condition of excellent (0.5 arcseconds) seeing. Because of the wavelength dependence of seeing, wider bandpass can be used at longer wavelengths. Further experiments are required to fully determine the optimum bandpass for speckle interferometry under specific seeing conditions.

For larger observing bandpass it is necessary to accurately compensate for atmospheric dispersion errors. Figure III.7a shows the result of observation of ADS 9744 with 30 nm bandpass at 550 nm at about 30^o from the zenith with no dispersion

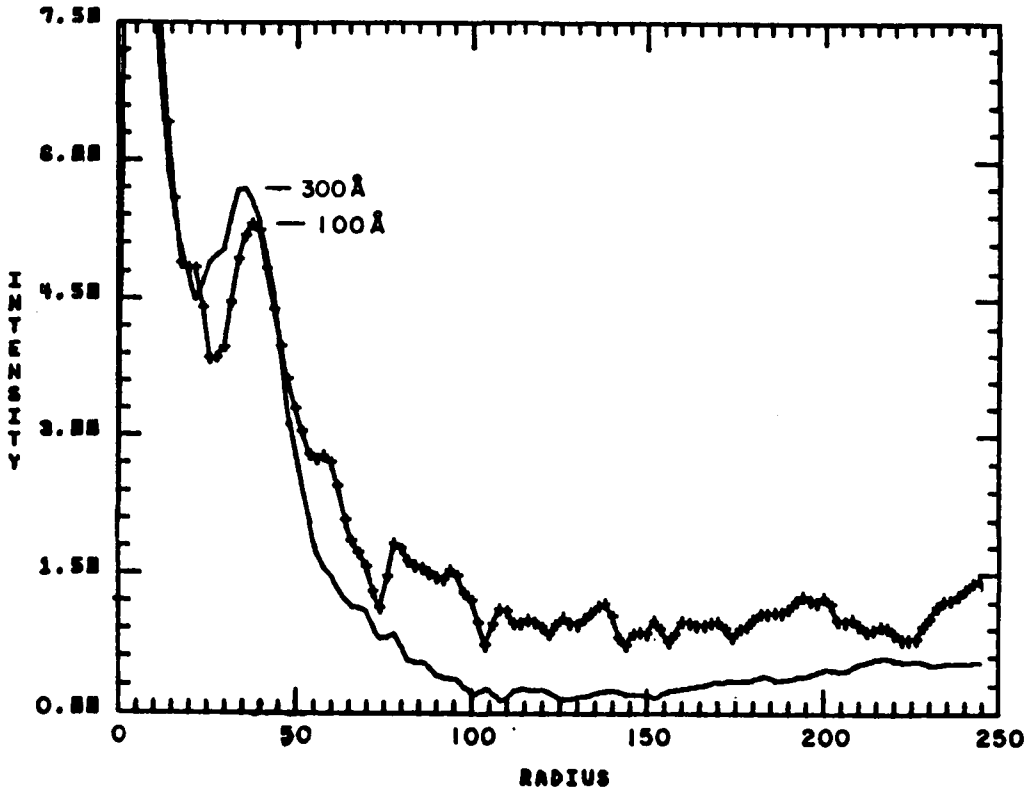

Figure III.6. Effect of observing bandpass. Loss of contrast is observed in the autocorrelation profile of ADS 9744 for the wider bandpass at 550 nm. (Seeing was 1.5 arcseconds)

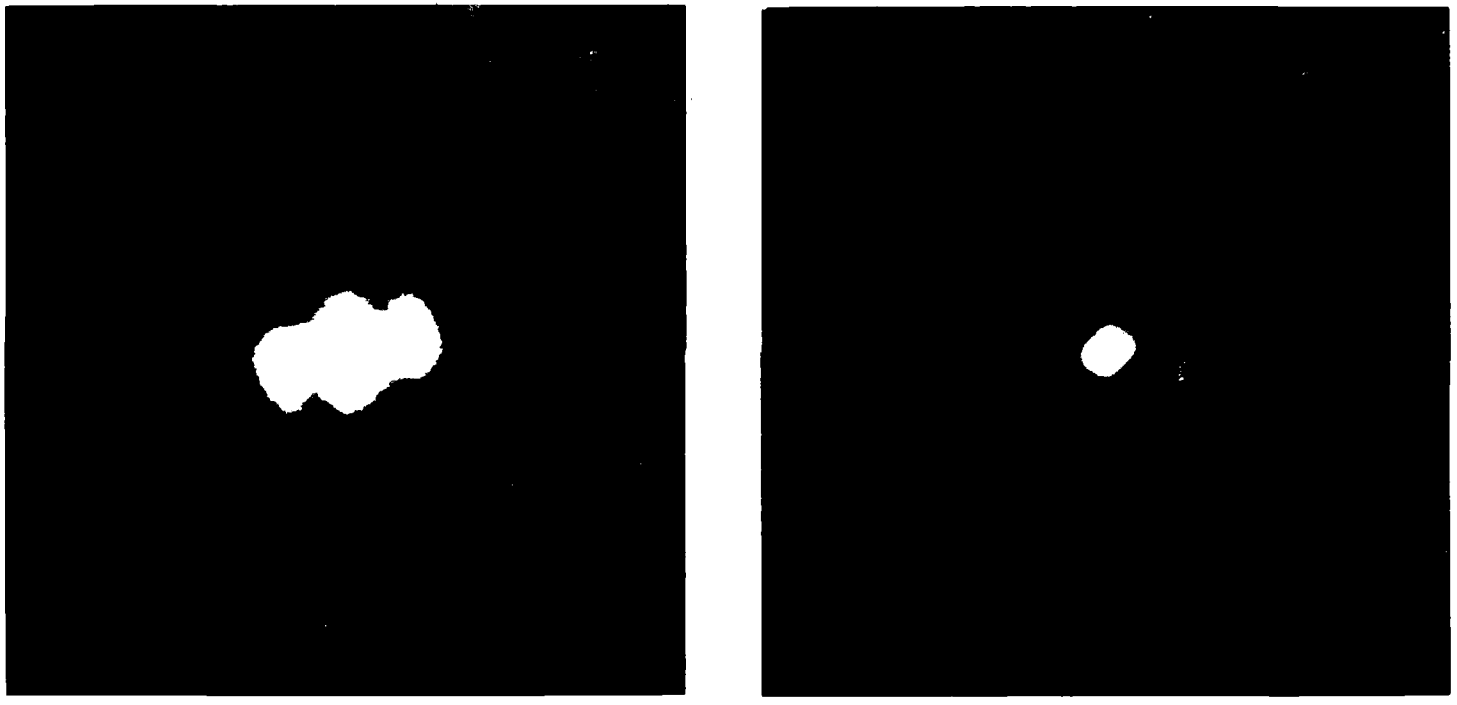

Figure III.7. Effect of anti-dispersion prisms. Seeing-corrected autocorrelation functions for ADS 9744 observed 30° from the zenith with 30 nm band-pass centered at 550 nm. (Left) No prism correction. (Right) Using anti-dispersion prisms.

correction. The elongated images are clearly evident. Figure III.7b shows a nearly optimized observation of the same star with 100 A bandpass at 550 nm using the antidispersion system.

III.C.4. Effect of Exposure Time

Speckle images of the binary star Kappa Ursae Major obtained using various exposure times from 5 ms to 40 ms were autocorrelated to observe the dependence of interferometric contrast upon exposure time. The seeing for these observations was about 1.5 to 2.0 arcseconds, rather typical for the 2.3 meter telescope. Figure III.8 shows that there were definitely observable changes in the atmosphere with time scales less than 10 ms, but that exposures as long as 40 ms still preserved some information at the diffraction limit of the telescope. This experiment does not show direct evidence for variations with timescales less than 5 ms, but they are implied by the fact that each factor of two decrease in exposure time produces a significant improvement in interferometric contrast.

The choice of 17 ms exposure time for our speckle camera is a matter of convenience (60 Hz video fields) and not a deliberate optimization of this parameter. Figure III.8 suggests that 5 ms exposures (200 Hz) would yield a factor of two improvement in the visibility of the ACF under typical seeing conditions, a speed which is not feasible with readily available commerical video components. Further experience suggests that this effect also is quite seeing dependent, and qualitative observations have

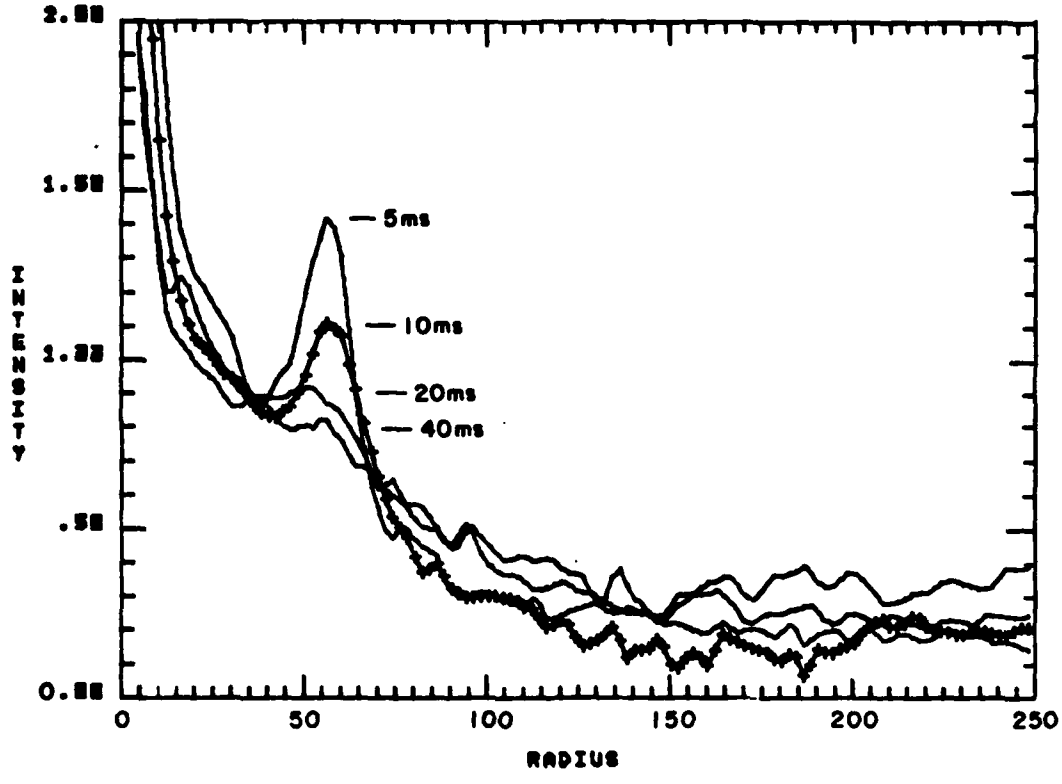

Figure III.8. Effect of exposure time. Radial intensity profiles of the seeing-corrected autocorrelation function of the binary star *UMa show increasing contrast with decreasing exposure time. (Seeing was approximately 1.5 arcseconds.)

shown that for good seeing some detectable information at the telescope diffraction limit is present in exposures as long as 1 second.

As for the effects of observing bandpass (section III.C.3), further studies are required to determing the optimum exposure time for speckle interferometry under specific seeing conditions.

III.C.5. Photon Statistics

For work at the faint object limit, the largest bandpass and longest exposure time possible must be utilized. The problem is one of photon statistics: in order to obtain information from a speckle image, such an image must be well populated with photons. For the faintest objects, this is the limiting factor. (See also section II.D.3.)

Consider the problem of detecting a binary star. For faint objects one may visualize the speckle image as that of a bright object but the intensity at any point (x,y) is now a measure of the probability of detecting a photon at (x,y), rather than a directly measurable amplitude, as for the very bright object. In order to produce interferometric information about a binary star, at least one photon from each component must arrive in a single speckle within the atmospheric correlation time, as argued in section II.D.3.

Dainty (1978) has given an analysis of this problem. Although not tested experimentally, we quote it here, as its qualitative dependence on photon statistics is consistent with our expectations based upon arguments such as the above.

$$\frac{S}{N} = \frac{\text{Signal}}{\text{Noise}} = \langle n_{ph} \rangle \quad \frac{n_{pict}}{2\langle n_s \rangle} \cdot \frac{\beta}{1 + 2\beta + \beta^2} \qquad \text{(III.4)}$$

where $\langle n_{ph} \rangle$ is the mean number of photons per speckle picture, and n_{pict}, is the number of speckle pictures. The total number of photons detected is $N = \langle n_{ph} \rangle n_{pict}$. The number of speckles (which may be estimated as the seeing disk size divided by the Airy disk size) is n_s and β is the binary star intensity ratio (I_B/I_A). This expression is valid for the faint object limit $\langle n_{ph} \rangle << \langle n_s \rangle$. For a binary star of large contrast, $\beta << 1$, this shows that the usual Poisson S/N = N is reduced by the factor

$$\varepsilon\ (n_{ph}, n_s, n_\beta) = \beta \quad \frac{\langle n_{ph} \rangle}{2\langle n_s \rangle} \qquad \text{(III.5)}$$

If the probability at a given point of detecting a photon originating from some resolvable element i on an object is P_i and the probability of detecting (independently) another photon originating from a different resolvable element j is P_j, then the probability of detecting photons from both resolvable elements at that point (i.e. within a given speckle) is $P_{ij} = P_i P_j$. Then for faint objects

$$\rho_{ij} = \frac{n_i n_j}{N^2} \qquad \text{(III.6)}$$

where n_i and n_j are the average number of photons per frame detected from elements i and j respectively and N is the average number of speckles per frame. For faint objects n_i and $n_j << N$.

The average total number of photons per frame is $n = n_i + n_j$ and the total number of photons detected is nF where F is the number of frames. The uncertainty in any observation of this number is $\delta(nF) = \sqrt{nF}$ and the uncertainty in the average n is $\delta n = \sqrt{n/F}$. For any given speckle, the uncertainty in the number of photons/speckle is

$$\delta n_i = \frac{n_i}{FN} \tag{III.7}$$

The corresponding uncertainty in the probability (3) is

$$\delta(\rho_{ij}) = \delta\rho_i \, \rho_j + \rho_i \, \delta\rho_j \tag{III.8}$$

and the signal-to-noise ratio is

$$\frac{S}{N} = \frac{\sqrt{n_i \, n_j}}{\sqrt{n_i} + \sqrt{n_j}} \sqrt{FN} < \sqrt{(n_i+n_j) \, FN} \tag{III.9}$$

For equally bright stars $n_i = nj = 1/2\ n$ so that for two resolution elements of equal brightness, the signal-to-noise grows less than half as fast as for a single resolution element.

$$\frac{S}{N} = (\rho_{ij}) = \frac{1}{2\sqrt{2}} \frac{S}{N}(\rho) = \varepsilon \frac{S}{N}(\rho) \tag{III.10}$$

The general case yields $\varepsilon = 1/2\ \sqrt{2}$ if $n_i = n_j$, and the faint component limit approaches $1/\sqrt{n_i}$ if $n_i >> n_j$. In this limit the signal-to-noise ratio grows extremely slowly with increasing numbers of detected photons. That is, the detective quantum efficiency approaches zero as the ratio of intensities approaches zero for a pair of resolution elements of arbitrarily large contrast.

IV. Scientific Results Obtained Using Speckle Interferomecry

Most of this work has already been published. We summarize the principal results and how they relate to the objectives of this contract work.

IV.A. The "Triple" Quasar

The blue quasi-stellar object PG1115+08 was observed by Weymann et al (1980) to be triple with components of $\sim 16^{m}.2$, $\sim 18^{m}.1$, and $\sim 18^{m}.5$ separated by 2-3 arcsecs. High resolution, long exposure images using image centroiding techniques (cf. III.C.1 and Figure III.1) indicated a somewhat elongated structure for component A. This object was accordingly observed at the MMT with speckle techniques. It became clear that the A component consists of two unresolved sources separated by 0.54 arcsecs at PA 20o. The "triple" QSO is thus at least "quadruple" in nature. If it is assumed that this multiplicity is due to the gravitational lens effect, arising from an intervening galaxy, the theory suggests that a faint 5th image should be present. The observations also show evidence of correlations between the fainter components (B and C) and component A (Hege, et al 1981). This is an example of "speckle holography" and shows that speckle observations of objects with components as faint as 18th magnitude can be carried out using even a 1.8m telescope. The work on PG1115+08 is of major importance for USAF studies of faint earth orbiting satellites in that it demonstrated that the technique of speckle interferometry certainly works for much

fainter objects than, for example, on-line wave front correction methods.

IV.B. The Pluto/Charon System

The planet Pluto was recently discovered by Christy and Harrington (1978) to have a faint companion, since called Charon. This discovery was of particular importance since it permitted, for the first time, an accurate mass determination for the system. The orbit is, however, highly elongated as projected on the sky at present so that speckle techniques become crucial in determining accurate orbital parameters; they also permit direct measurements of the angular diameter of Pluto and Charon. This work, (Hege et al, 1982b) yielded revisions to the epoch of the orbit and to the inclination of the orbital plane and, hence, to the predicted onset of eclipse. The measured angular diameters of Pluto and Charon were determined to be 0.14 (±0.02) arcsecs and 0.05 (±0.03) arcsecs respectively. On the basis of these results and estimates of relative total brightness, it appears that the two objects have similar albedo.

IV.C. Betelgeuse (Alpha Orionis)

Observations of α Ori, a red supergiant, have been made at a number of wavelengths in order both to determine size and shape parameters and to attempt real image reconstruction. Our results are as follows:

a) In the continuum the size of α Ori increases toward shorter wavelengths, confirming some earlier suggestions. The size at 6,000A is approximately 0.050 arcsecs.

b) The projected continuum shape is not circularly symmetric.

c) Reconstructed images suggest that the asymmetry is due to a bright star spot at position angle 205°.

d) The size of α Ori in H_α light is at least a factor of 5 larger than in the adjacent continuum, with evidence for emission up to 0.25 arcsecs. This corresponds to the distance at which strong thermal infra-red emission begins a phenomenon thought to arise from dust formation. α Ori is asymmetric in H_α emission also.

e) The asymmetries in shape may vary in time and appear to be correlated with changes in polarization. These variations are consistent with polarization arising from a scattering process in a stellar wind.

Further data have been gathered on α Ori which should confirm the image reconstruction result; reductions are currently in progress. Data has also been obtained in the Ca^+ infra-red triplet. A summary of preliminary results on α Ori has been published (Goldberg, et al. 1982).

IV.D. Observations of Asteroids

Observations of numerous asteroids have been carried out at the 2.3m and 4m telescopes. Most of these are still in the analysis phase but the following preliminary summary of results can be given.

a) Angular diameter measurements have been made for the four brightest asteroids: Vesta, Juno, Ceres, and Pallas.

b) Among these, Vesta shows clear signs of surface structure while Pallas appears to be elongated and is possibly binary. This latter result is consistent with light variations exhibited by Pallas. A preliminary announcement of this result has been reported (Science News, November 1980 and Hege, et al., 1980b, 1980c,) and includes estimated diameters of 550 km and 175 km for Pallas and its satellite, respectively. A series of systematic observations of Pallas, following its rotation, is now being analysed.

c) Observations have been made of other asteroids which exhibit short period light variations; the purpose is to search for possible binary systems and to determine structural parameters of the systems. So far in addition to Pallas, Metis and possibly Victoria may show signs of duplicity.

d) Programs have been developed to determine the semi major axes and spin directions of rotating ellipsoids from observations of their projection on the sky. These programs are being applied to asteroids; work on Eros is approaching completion. These techniques could be of considerable utility in analysing basic shape parameters for earth orbiting satellites.

The data on asteroids are now being re-analysed using our improved reduction techniques, after which it will proceed to publication.

V. Speckle Interferometry for High Resolution Imaging of Earth-orbiting Satellites: Present Status and Future Prospects

To put the effects of "seeing" caused by turbulence in the Earth's atmosphere on scale, we present in Table V.I. the linear size of seeing and diffraction limited images for a variety of telescopes and satellite ranges.

TABLE V.I. Satellite Resolution Limits

Telescope Diameter	Diffraction Limit	Approximate Resolution Limit 200km(LEO)	10000km	10000km(HEO)	Altitude 40000km (synchronous)
Seeing Limit	1"	1m	5m	50m	200m
60 inch (Maui)	.075	.05	.25	3	10
2.3m (Steward)	.05	.03	.25	2	7
4m (Kitt Peak)	.03	.02	.10	1	4
7m (MMT)	.017	.01	.06	.6	2

It is apparent that satisfactory resolution is achieved in Low Earth Orbit (LEO) with only modest image quality improvements over the seeing limit, and for this other methods (e.g. image enhancement either by post processing or by active optics systems) are probably appropriate. However, High Earth Orbit (HEO) satellites, at altitudes a sizable fraction of geosynchronous (40000km), are barely resolvable even at the diffraction limit of the largest existing telescopes. For this

reason methods such as optical speckle interferometry which can exploit the optical diffraction limit must be used to get HEO satellite images.

For LEO objects, specially constructed telescopes, such as the Maui HI AMOS/MOTIF 48 and 60 inch instruments, are used for imaging. These telescopes are optimized for rapid tracking and are located in good seeing sites with additional attention paid to minimizing local atmospheric turbulence to further enhance image quality. Recently, active optics have been added to the Maui 60 inch to further improve image resolution.

For HEO satellites doppler radar imaging has been used. This provides resolutions on these objects of better than a foot. However, this approach requires the target satellite to be rapidly rotating. With increasing numbers of three axis stabilized satellites at all altitudes, interest has risen in using speckle interferometry as an alternate means for HEO satellite imaging.

Astronomical telescopes are not designed for the rapid or non-equatorial tracking required for most satellite observations. The Steward Observatory 2.3 meter, for example, can not accurately track at rates much faster than several arc minutes per second of time. As seen in Table I, HEO satellites can not in general be well resolved by the 2.3 meter, and it cannot track an object much lower than 10000km. For this project it was therefore necessary to pick a large object at a suitable altitude. With the help of the Air Force Foreign Technology Division (FTD), we chose a Soviet Molniya communications satellite as a test target. This object is relatively large and

has a 12 hour orbit. This meant that it traversed a range of altitudes between synchronous and LEO. At about 10000-20000km we were able to both track and resolve this satellite. (See section II.E. and Worden, et al. 1979).

Noting the limited utility of the 2.3 meter telescope for HEO satellite imaging, we began in this program to use the MMT for tracking and imaging satellites. The MMT has two advantages for satellite work. Besides its obvious increased resolution limit, its mounting design is capable of tracking at at least ten arc minutes per second. This means it can track satellites down to about 1000 km altitude where even a single 72 inch component mirror of the MMT provides usable high resolution images.

V.A. Acquisition and Tracking of Non-Sidereal Objects

V.A.1. Tracking Rate Requirements and Present Capabilities

Just before he left FTD in September 1979, Col. Feaster generated for us an "ideal" observing ephemeris for a hypothetical MMT speckle interferometry observing run. This ephemeris included objects with mean observing ranges less than 2000 km. The list of objects was

1. Salyut 6
2. Cos 1076
3. Meteor 2-4
4. Cos 1116

for observing dates 21-23 September 1979. Upon review of this ephemeris, we concluded that none of these objects could have been observed with the MMT tracking capabilities existing at that

time. The following summarizes the considerations leading to that conclusion, and serves to define the problem against which we are evaluating our present capabilities.

Table V.II. summarizes the rates for one of the slowest of these, Meteor 2-4.

TABLE V.II. Satellite Rates

Range	Rate	Elevation	Interval
1800 km	10^{o}/min	20^{o}	7.5 min/crossing
1000 km	26^{o}/min	52^{o}	9.5 min/crossing

From this we conclude that tracking capabilities up to 30^{o}/min = 1800"/sec are required for such an object. Present 2.3 meter telescope capabilities are about 200"/sec, which misses by about a factor of ten. This is what limited us to the Molniya observations discussed in section II.E.

Slow moving objects have been observed in the wide-field video acquisition system, described below in section V.A.2, using the MMT. Due to an unfortunate combination of circumstances, including miscommunication of data and inclement weather, no satellite observations have been made using the speckle camera with the MMT. However, much has been learned from an analysis of the performance of the MMT mount control system parameters while tracking such slow moving objects. Quite acceptable error values (< 0".3) are found for velocities up to 120"/sec. This is adequate for objects beyond 20,000 km range. The tracking errors increase with increasing tracking rates. For the intermediate range, 5,000 km to 20,000 km, the present

tracking errors appear to approach 1" for object rates approaching 500"-600"/sec. This is still a factor of three less than that required for a Meteor 2-4 observation, and nearly a factor of ten less than that required for a rapid object like Salyut 6 which, in the case examined, reached rates of nearly 4500"/sec at an elevation of 62°, (range 430 km) and required only 3.5 minutes for the crossing.

V.A.2. Acquisition of Objects with Inaccurate Coordinates

Experience with ephemerides supplied to us by FTD has shown that the predicted positions for the objects depart from the actual positions at which they are found, often by as much as 1 to 10 arc minutes. Thus a wide-field acquisition system is required. For the measurement described in section II.E., the satellite was acquired visually using the 10 inch refractor associated with the 2.3 meter telescope. For wide-field acquisition at the MMT, we have installed an 8 inch Celestron telescope attached to a Steward Observatory designed image intensifier/television system. This capability is useful to detect and acquire objects as faint as visual magnitude 12-14, depending upon sky brightness, in a field of view of approximately 30 arc minutes diameter.

V.A.3. Tracking Software for Telescope Drives

Ephemeris Reformatting

The ephemerides supplied to us by FTD are written on 9-track magnetic tape as ASCII characters. Before they can be used by the mount control systems they must be translated into FORTH

compatible binary form. The satellite's apparent right ascension and declination (for the 2.3 m telescope) or azimuth and elevation (for the MMT) are tabulated at approximately one minute intervals. Periods of visibility lasting anywhere from a few minutes to all night are detected by the program. A header block containing pertinent identifying information is generated for each visibility interval followed by a table consisting of UT and the two corresponding angular coordinates appropriate to the particular telescope. The UT is a 32 bit integer in milliseconds and the angles are 32-bit integers in units of 1/20th arc second. This reformatted information is then written back on 9 track tape for use by the telescope control systems.

We note that the most difficult aspect of the satellite testing has been getting a target tracking tape from FTD with current coordinates and with enough time to get the tape to the telescope prior to the observing run. This same problem has plagued our efforts to adapt the MMT to satellite tracking. Nevertheless, we have been able to successfully track satellites with both the 2.3 meter and the MMT. We are confident that we can now use either telescope as required in future satellite studies.

The 2.3 Meter System

This tracking program uses the system clock to linearly interpolate the position in real time and drives the telescope accordingly. The present system does not know the actual telescope coordinates, so these must be initialized appropriately by the observer. The ephemerides gives apparent coordinates. Therefore, a star with accurately known coordinates near the

point at which tracking is to begin is set accurately in the detector field. Then the program computes the offset from the known coodinates of the reference star to the initial ephemeris position and moves the telescope accordingly. There are two tracking modes. The first is appropriate if ephemeris errors are small. It starts telescope tracking at the designated UT entered by the observer. Often ephemeris errors are larger in position along the predicted orbit (early or late). The second mode allows starting the tracking when the object is acquired while waiting in advance at a predicted position. In this mode the program UT is reset to the ephemeris UT at the time the object is actually acquired.

The MMT System

Since the MMT mount control system has available the absolute telescope encoder positions, the program is conceptually much simpler. A quadratic interpolation is used to drive the telescope along the predicted path. The coordinates can be entered only manually in the present system. However, one per minute is quite within the capability of the telescope operator. We have found that quadratic interpolation on 10 minute intervals appears adequate for Molniya type orbits, hence 1 minute intervals should continue to be adequate for the faster moving objects. To accommodate ephemeris errors, the system allows manual guiding to place the object in the detector field and then to continue tracking along a path parallel to the ephemeris path. The program can add offsets to UT to accommodate objects which are early or late.

It should be a minimal program modification to allow entry of program coordinates from a floppy disk written as previously described under Ephemeris Reformatting.

V.B. Real-Time Data Capture and Reduction

We believe we now have ample evidence to justify an on-line, real-time event-capture system. We have used the present software realization of this system to measure object shape parameters directly from deconvolved power spectra and hence to obtain major-axis, minor-axis and position angle for asteroid images assuming uniform disk illumination. Noise models appear to be valid only for first-order correction of power spectra noise bias. However, data taken without independently measured noise bias appear to be noisy, or too poorly calibrated to justify any attempts at fitting intensity profiles which depart from uniform disk illumination. These studies suggest the following system and procedural requirements.

1. Video-Tape-Recorders must be eliminated from the data acquisition system. They introduce large systematic effects which are nearly impossible to calibrate.
2. High-quality calibration data are required.
   a) A standard star (point source) must be observed with good statistics by chopping back-and-forth between standard and object to assure that any changes in seeing are properly tracked.
   b) Detector transfer functions must be measured to properly remove noise bias. This must be done with a linear,

direct-coupled system. Non-linearities in VTR's are the limiting factor in the present scheme.

Software which works quite well to extract magnitude differences for binary stars from simulated data sets, even when a large amount of Poisson noise (photon statistics)is added, fails to give valid results for magnitude differences for faint-object (photon-event mode) reductions of real binary star data. The limiting systematic effect, which continues to defy calibration given our present video-taped data base, appears to be the detector transfer function and its effect in coloring the noise bias in a data-dependent way.

On-line data reduction capabilities are essential to this project for two further reasons:

1. Real-time fringe-contrast detection is needed for optimal phasing of the various interferometric paths in the MMT. It is expected that shifts in the telescope configuration with time (flexures induced by temperature drifts and thermal gradients) and elevation (gravitationally induced flexure), although gratifyingly small in our preliminary studies (see section II.G.), will inevitably require readjustment of the interferometer. Since each of five independently phasable telescopes must be compared to the sixth, used as a reference, it is essential that a capability to quickly and accurately make these adjustments be implemented.

2. The ability to produce a size and shape estimate immediately upon completion of an observation with no further investment of time for off-line computations is ultimately of particular relevance for Air Force applications.

V.B.1. Hardware Requirements

An orderly progression of increments in capability should lead ultimately to computation in real-time at the observing site of seeing-corrected speckle autocorrelation functions. In hardware, the progression beyond the implementation of Video Differencecapability, already accomplished,(section II.B.) includes

1. Camera stabilization and synchronization.
2. Event detection hardware for localizing photoelectron events to single pixels along the raster lines.
3. Computer interface for event detection hardware.
4. Event detection hardware to include event centroiding capabilities for localizing photoelectron to unique raster line (1/2 TV scan-line resolution).

At stage 4, the hardware will have the capability of registering photoelectron events as unique single-pixel events in a 480 x 512 pixel format at 60 Hz frame rates using a standard repeat-field (*non*-interlaced - 240 line) format.

V.B.2. Software Requirements

Existing parallel capabilities in software should be similarly expanded in on-line realizations to produce

1. Autocorrelation functions from event address lists.

2. Methods for applying seeing corrections.

3. Event centroiding. Software realizations of centroid determining algorithms will be used to determine an appropriate design for the hardware implementations.

4. Suitably optimized algorithms for real-time execution.

Presentlty, all four stages of the software development have been demonstrated. Successful methods for producing seeing corrected speckle autocorrelation functions from event address lists have been demonstrated. A two-dimensional event centroider has been realized in software and used to localize events detected as covering several pixels, splotches recorded in 240 x 256 format, as single pixel events in 480 x 512 format. Seeing corrected speckle autocorrelation functions computed from the resultant centroided event lists have shown the expected properties. A binary star power spectrum produced by this method is shown in Figure V.1. Optimized algorithms have been written for use in a reduced 128 x 128 format which, when running in existing observatory minicomputers, can keep up in real-time with modest signal rates (about 100 events/frame).

V.B.3. Plan for System Improvements

Hardware capabilities at present are less well developed. Grinnell Video Digitizers with Video Difference capabilities have been acquired for use at both the 2.3 meter telescope and the MMT. Camera synchronization and stabilization must be implemented. The event detection hardware necessary to implement the full capabilities manifest in the Grinnell Video systems will

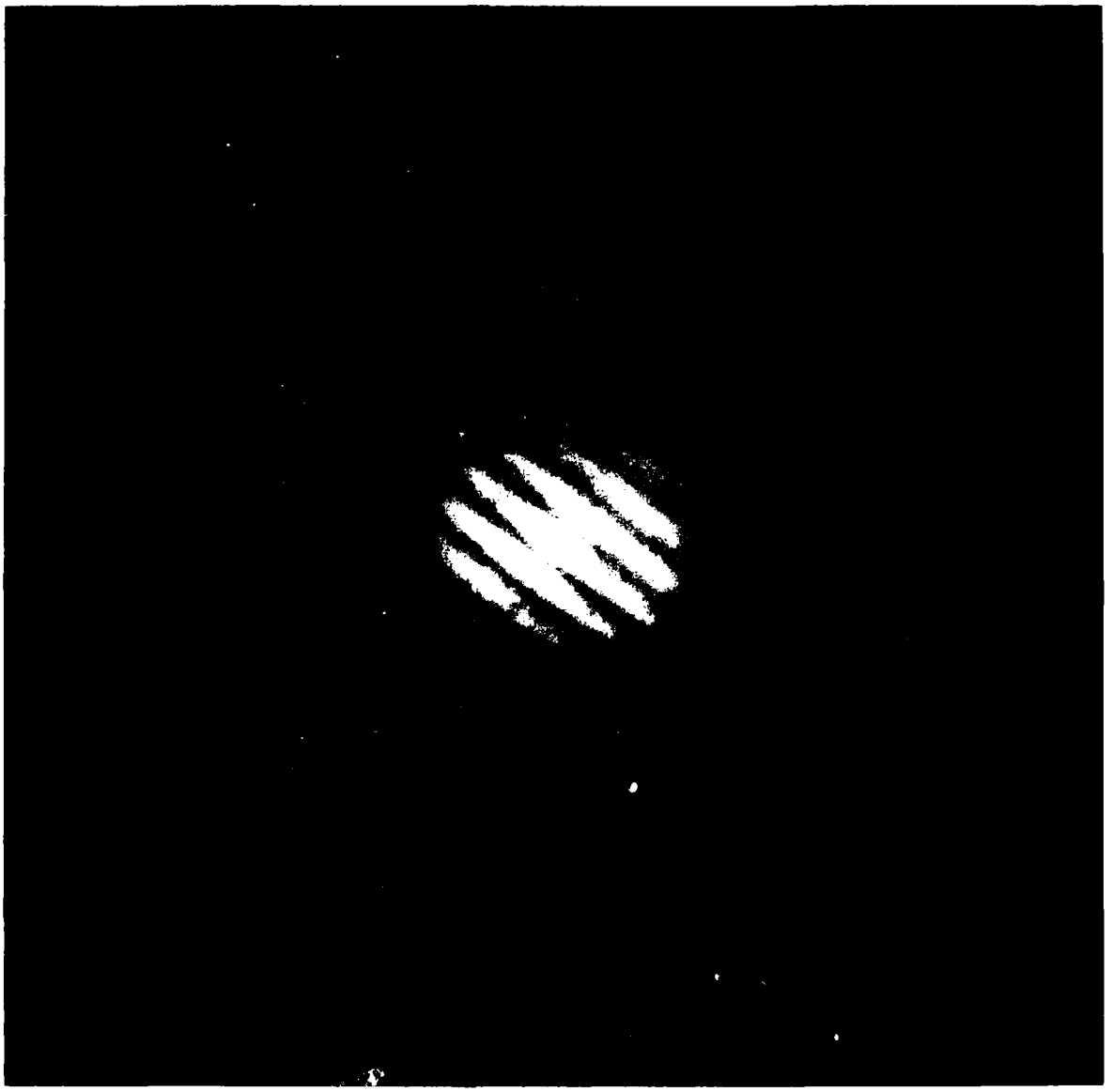

Figure V.1. Seeing-corrected power spectrum for SAO 94163 produced from event-centroided data. The noise bias is nearly uniform except at image frequencies higher than the aperture diffraction limit.

be designed and built with Steward Observatory engineering and fabrication capabilities.

We expect to implement these systems in two stages:

1. One-dimensional event centroiding

For one-dimensional centroiding to one-pixel precision, the stability of the combined camera-digitizer system must be such that no relative drifts as large as one pixel can occur. Upon completion of the hardware to localize each event to a single pixel along a raster line and an appropriate computer interface to output the element address together with its associated line number, the one-dimensional on-line capability necessary to compute one-line dimensional sharpness functions in real-time, can be implemented immediately with existing software.

2. Two-dimensional event centroiding

We expect that with a three-line circular buffer a hardware processor to localize an event multiply detected on adjacent scan lines can be implemented to produce unique photoelectron addresses. This will allow the immediate implementation of 128 x 128 autocorrelation functions computed from a sub-matrix of the 480 x 512 detector format. The limitation on the array size arises from limitations in the memory capabilities of thepresent minicomputer systems at the observing sites. (Three n x n arrays must be kept in memory for the computation of a 2n x 2n seeing corrected autocorrelation function). Larger autocorrelation functions will require larger minicomputers or dedicated hardware processors and associated memories. The 128 x 128 format is adequate, however, to sample objects of small extent (0.5 or

less) at the aperture limit of the MMT. Such a small format will not be able to sample the full isoplanatic patch at the full resolution of the MMT, however.

We can now specify the components of a system with capability of producing on-line seeing-corrected autocorrelation functions in 480 x 512 format. The system must be able to record on-line with 100% duty cycle and at up to 1,000 events/frame, the entire 480 x 512 format for off-line processing to exploit the full image resolving capability of the MMT. The fast autocorrelation algorithm requires a word-length of at least 18 bits to accomodate the 480 x 512 data format on-line, and hence is, beyond the capabilities of present Steward Observatory minicomputer systems.

At present, the TV camera is clocked independently to the Video-memory. This results in frame to frame synchronization problems which to some extent compromise the performance of the subtractions of background and phosphor glow build-up, especially in the photon counting mode. To correct this, we plan to modify both the camera and the memory to function on a common external clock.

The SO/AFGL detector is, to our knowledge, unique among intensifier/TV systems in that it already provides for frame to frame subtraction to preclude repeated counting of a single event (see Section II.B.). This is essential in speckle work if frame to frame correlation is to be minimized. We have carried out a study of the pulse height distribution of the detector system and have shown that the interframe difference signal is highly suited to unitizing (Hege, et al. 1980a).

In summary, we expect to:

1. Implement a single frame readout mode (i.e. eliminate the standard video frame interlace).
2. Provide line-centroiding logic which will permit events to be localized first to a precision of 1/2 analogue resolution element (1 in 500 pixels) with possible later extension to 1/4 element (1 in 1,000 pixels).
3. Provide line-to-line event centroiding with closely similar resolution properties.

The resultant output will be addresses of photon events -- an ideal form for rapid computation of autocorrelaion functions, etc. It is clear that at the low light levels typical of work on artificial satellites, as well as most astronomical sources, the event detection mode is the appropriate way to proceed. For this mode, it is a great advantage, from the points of view of sampling, signal to noise and speed of reduction, to centroid and unitize each detected photon-event.

With such an on-line system at the MMT, it should be possible to produce initial estimates of shape and size of an object within minutes of the completion of an observation. This is an important consideration for observations of any target of military significance.

V.C. Detector resolution and diffraction limited image sampling

For a telescope of 6.9m aperture and λ = 500 nm, λ/d = 15 millseconds of arc (msa). To adequately sample the speckles to produce diffraction limited (rather than diffraction + detector limited) results it is necessary to oversample. Practical

experience dictates a further factor of two in sampling resolution over that predicted by the Nyquist theorem in order to sample the diffraction limited speckle profiles with good fidelity. Thus we require

$$\Delta x = \frac{\lambda}{4d} = 4 \text{ msa}$$

Upon occasion seeing better than 0.5 arcseconds has been measured for short exposure speckle images. However, a detector field several times larger than this is required to exploit such conditions, as this seeing is superimposed upon a nearly comparable component of image wander. For all applications in which good signal to noise depends upon good photon detection efficiency, it is necessary to keep the image well centered in the field on the average, i.e. the detector must be large enough so that the instantaneous image is within the detector view. Thus detector fields of at least 1.5 arcseconds are required for ideal seeing conditions. Practical experience has shown that 2.5 arcseconds is a reasonable minimum field size for good seeing conditions (well-guided images 0.5 to 1.0 arcseconds FWHM).

If a detector system with 480 by 512 pixels is operated at maximum resolution, the Nyquist resolution is 240 x 256 and the over-sampled resolution required for optimum fidelity is 120 x 128. This gives a maximum diffraction limited field of size L,

$$L = 128 \quad \Delta X_{diffraction} = 2 \text{ arcseconds}$$

using analogue detection methods. In the event centroided photon detection mode we expect to make the detector pixel frequency

match the Nyquist frequency in order to give an over-sampled resolution of 240 x 256. This gives a maximum field of 4 arcseconds which is adequate for most of the seeing conditions we have encountered.

For bright objects, one can afford to utilize small fields to explore the resolution of the aperture limit by letting the image spill outside the detector field. As the light losses are not intolerable the image centering problem is not crucial. For fainter objects, if the light is not well concentrated in the field, it is extremely difficult to achieve image centering, and the resultant losses of more than 50% of the light in signals already photon starved is intolerable. Furthermore, manual guiding, which is required for non-sidereal objects with only approximate ephemerides, is impossible if image intensity gradients are not preceivable in all directions in the field (i.e. if the image is not well contained in the field).

Summarizing, faint object experiments can only be accomplished with the present detector system by compromising the resolution of the aperture. A detector having the capability of resolving 800 line pairs in the video raster - 400 detector analogue resolution elements is required. When operated at an image scale such that the field is 1.5 arcseconds, this produces just the required ΔX = 4 msa. The physcial resolution is 37.5 μm along the 15 mm television raster which corresponds to 62.5 μm at the image intensifier photocathode. We note that only an on-line implementation of such a detector will not be subject to the limitations of the video tape recorder electronic bandpass. This detector is the minimum required to implement reliably an

observation of a non-sidereal object of 10-12 magnitude brightness while exploiting the diffraction limit of a 6.9 meter optical baseline.

VI. Speckle Interferometry for Scientific Investigations

VI.A. Resolved Stellar Systems, Galactic Nuceli and QSO's

(a) Supergiant Atmospheres

Supergiant stars, such as Alpha Orionis, are characterized by high luminosity and low surface gravity. Their atmospheres are extended both because the atmospheric scale height is comparable to the stellar radius (i.e. the photospheric radius is not well defined) and because they usually show evidence of stellar winds and, hence, mass loss. An improved understanding of the structure of supergiant atmospheres is important in a number of astrophysical contexts, including stellar evolution, the chemical processing of the interstellar medium, and the generation of stellar winds and coronae. Significant progress can be achieved by measuring the diameter of supergiants as a function of wavelength, since the results depend directly on the temperature stratification and the opacity. In this manner it should be possible to derive important information on the temperature and density distributions in the atmosphere, to determine whether the mass outflow is spherically symmetric in the atmosphere. The approach should also permit us to locate the region of wind acceleration and perhaps to derive important data on the process of dust formation.

(b) Pre-Main Sequence Binaries

The masses of pre-main-sequence objects can be determined directly by observing the orbital motion of close binaries using speckle interferometry. The techniques are

identical to those used with considerable success in st[illegible]ies of main-sequence binaries by us and other groups; the objects are, however, faint.

Binaries with separations of 0.05 arc-sec, located in nearby (R = 100 - 150 pc) star formation regions like the Taurus-Auriga dark cloud, have orbital periods of about 10 years. In many cases the observation of a quarter of the orbit should be sufficient to calculate reasonably reliable orbital elements. This means that it is in principle possible to determine the masses of nearby pre-main sequence objects within a few years.

(c) White Dwarf Mass Determinations

Measurement of the masses of highly evolved stars is likewise in a very primative state. Good mass determinations presently exist for only three white dwarfs: Sirius B, Procyon B and 40 Eri B - all from direct binary orbit measurements and all for spectral type DA.

Speckle interferomic obsevations should be carried out on nearby white dwarfs, especially those suspected to have an M dwarf companion, in order to identify binary systems and determine individual masses.

(d) Active Nuclei of Galaxies

The nuclei of galaxies consist of high surface brightness, unresolved ($\theta < 1$ arcsec) knots of emission. In the case of certain elliptical galaxies (e.g., M 87) the nuclear emission appears to be primarily due to late type stars. In others, especially the Seyfert galaxies, the radiation appears predominantly in broad emission lines and in a non-thermal

continuum; these nuclei appear to be closely similar to the QSOs. Many lines of evidence suggest that most powerful extragalactic radio sources originate in active nuclei of galaxies. The nature of the processes taking place in such nuclei are, however, not yet understood. Among questions to be answered observationally are:

(1) What is the angular extent of the non-thermal continuum source, the stellar core and the broad emission line region? Light variation data suggest that the non-thermal source size is generally well beyond present speckle interferometric capabilities, but it is still important to set limits. The stellar cores and broad emission line regions should be resolvable in at least the closer Seyfert galaxies. Indeed, data already obtained in the H_α line for NGC 1068, the prototype Type 2 Seyfert, indicate that the nucleus consists of numerous small clouds dispersed through a region extending $\sim$ 1 arcsec.

(2) Is there evidence for systematic structure in the continuum or line radiation which might be the consequence of, for example, the accretion disk hypothesized to be responsible for the energy sources in these active nuclei?

(3) Does the structure observed in the emission lines relate in any way to that observed at radio wavelengths? There is, for example, now ample evidence from QSOs that the measured (VLBI) sizes of the compact radio cores are comparable to those inferred indirectly for the emission line regions.

(e) QSOs and Gravitational Lenses

So far three QSOs have been discovered which appear to consist of multiple but identical images and thus constitute

likely examples of the effects of gravitational lenses. The lensing objects are thought to be an elliptical galaxy and the cluster of which it is a member in the case of the "double" QSO 0957+56 and a spiral galaxy in the case of the "triple" QSO 1115+08. Clearly the frequency of lensing and the resultant image characteristics provide a wealth of data on the nature of the material causing the lenses. A survey is thus already in progress aimed at detecting further cases at relatively wide separation (> 1 arcsec). It appears likely, however, that such lenses should not result only in images separated by more than 1 arcsec. Indeed the brightest component of the "triple" QSO has already been resolved by speckle interferometry into further components separated by 0.54 arcsec. It is thus important to carry out at least a limited survey of QSOs to search for such structure.

VI.B. Speckle Polarimetry

Polarization measurements have often proved of immense importance in astrophysical studies. This appears to be true for supergiant atmospheres, stars which are still undergoing formation, and the nuclei of active galaxies. In the case of supergiant atmospheres, polarization is expected to occur as a result of resonance line, Rayleigh or dust scattering in the envelope. This can in principle be measured using speckle polarimetry, and in turn provides a check on the opacity and structure of the atmosphere. Such measurements should be of still greater value in studying the envelopes of newly forming stars or those that are undergoing a prolonged mass loss phase.

The data provide information on both the central source and the degree of locally generated emission.

Finally we note that the nuclei of Seyfert galaxies (e.g. NGC 1068) are often polarized in a manner suggestive of scattering in circum-nuclear dust envelopes. This may in turn be related to the accretion disk and mass outflow structure postulated earlier. High resolution polarization measurements should provide a means to test the various models.

VI.C. Validation of Speckle Image Reconstruction Techniques

The standard output of speckle interferometry is an autocorrelation function which contains diffraction limited information on the object. It does not in general provide a diffraction limited image, although in certain special cases, for example, when there is a point source within the isoplanatic patch, such information may also be present.

A number of image reconstruction tests on real data are required for validation of the processes for image reconstruction studied under this contract. Principle goals should be to demonstrate that:

(a) Accurate relative brightness data can be derived from speckle observations of binary stars. This represents the simplest possible extension of the basic structure information (separation and position angle) which may readily be derived from autocorrelation analysis. The results should be compared with results derived from occultation measurements and from analysis of the autocorrelation functions -- as opposed to using the above

image reconstruction methods. The study should be carried out for a range of magnitude differences.

(b) The basic brightness variations across the face of one or more Jovian or Saturian satellites can be accurately reproduced by speckle techniques at the diffraction limit of the telesocpe used. Candidate satellites include Io and Iapetus both of which have solid surfaces with substantial brightness contrast and negligible atmospheres. Both subtend angles smaller than a seeing disk, yet have an adequate number of resolution elements across their face. These efforts should concentrate on deriving the correct basic structure and accurately retrieving the surface brightness levels.

VI.D. Speckle Image Studies

The success of the various speckle analyses depends to a considerable extent on selection of optimum observing parameters such as exposure time, bandwidth, and wavelength, among others. This selection in turn depends on the scientific problem in question, the telescope, the atmospheric properties at the time of observation, etc. While the qualitative effects of these various parameters are better understood as a result of this contract work, there is still much to be learned about their quantitative influence on the speckle results and hence on observing strategy. Our preliminary studies of these questions should be extended to a variety of atmospheric conditions and telescopes.

Specifically, the program should include studies of:

(a) the effect of telescope focus and aberration on speckle MTF;

(b) the effect of exposure time on speckle MTF as a function of wavelength; atmospheric conditions (seeing) and observing bandwidth;

(c) the effect of bandwidth on speckle MTF as a function of atmospheric conditions, wavelength and exposure time;

(d) the distribution of energy among the speckles as a function of wavelength, bandwidth and telescope size;

(e) the dependence of autocorrelation function signal to noise on photon rate and wavelength: this leads to a determination of the limiting magnitude for useful speckle applications;

(f) possible parameterizations of the seeing contributions to the speckle MTF and the degree to which these can be determined from observations of the program object.

AD-A120 410 IMAGE RECONSTRUCTION USING LARGE OPTICAL TELESCOPES(U) 2/2
STEWARD OBSERVATORY TUCSON ARIZ E K HEGE ET AL.
15 FEB 82 AFGL-TR-82-0136 F19628-78-C-0058

UNCLASSIFIED F/G 20/6 NL

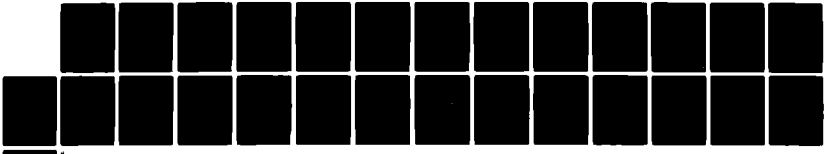

END
DATE FILMED
2 83
DTIC

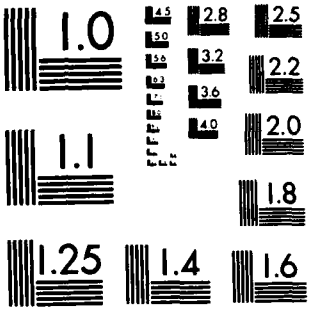

MICROCOPY RESOLUTION TEST CHART
NATIONAL BUREAU OF STANDARDS-1963-A

VII. Abstracts of Publication

1. DIGITAL SPECKLE INTERFEROMETRY TO MEASURE THE ANGULAR DIAMETERS OF FAINT OBJECTS

G. Hubbard, K. Hege, M. Reed, P. Strittmatter, S. Worden
In I.A.U. Colloquium #50, Paper 28 (1979).

We have developed a digital speckle camera for use on the University of Arizona 90" telescope. This camera uses a CID detector to provide photon locations in an image, or an analog image for brighter objects. We have used this system to observe Saturn's satellites Rhea and Iapetus. Using a correlaion speckle technique, we have determined the angular diameter of these objects to be 1487 ± 40 km for Rhea, and 1200 ± 132 km for Iapetus.

2. SPECKLE INTERFEROMETRY I. THE STEWARD OBSERVATORY SPECKLE CAMERA

E. N. Hubbard, E. K. Hege, M. A. Reed, P. A. Strittmatter, S. P. Worden, Astron. J., 84, 1437 (1979).

The Steward Observatory speckle camera is described. The optical system images light onto a four stage image tube which is then lens-coupled to either a photographic camera or to a CID camera. The device has been used in its photographic mode to study the extent of the iso-planatic patch at the 2.3m telescope. With 30 m sec exposures, the correlation between the speckle patterns of close binary systems has essentially disappeared for separations exceeding 6 arc secs.

3. DOME SEEING

N. J. Woolf, Pub. Astron. Soc. Pacific, 91, S23 (1979)

A theory of dome seeing and its relation to dome heat sources is developed using the mixing-length theory of convection. Comparison with limited observations and experimentsin the literature encourages hope that it is numerically approximately correct. The paper specifically studies heat sources that result from the telescope and dome responding to diurnal temperature variations and frontal passages. It is concluded that current designs and uses have problems, and that as telescopes are made larger these problems would become worse. Some solutions are proposed.

4. THE FUTURE OF GROUND-BASED HIGH RESOLUTION IMAGING

N. J. Woolf, Ann. Rev. Astron. Astrophys. (1982)

It is well known that for many purposes the power of a telescope is proportional to the primary collecting area divided by the solid angle formed by the images, and thus a 2.5m telescope with 0.5" images is equivalent in performance to a 5m telescope with 1" images. A substantial part of the funds available to ground-based astronomy are spent on the construction and operation of large telescopes. Since the power of these telescopes in inversely proportional to the image solid angle, it would seem as worthwhile to shrink images as to build large telescopes, yet there is a clear disproportion in the amount of effort and funds spent in these two areas. There is also a disproportion in the amount of easily accessible information available in the literature to guide the astronomer.

Although large telescopes do,on rare occasions, produce small images, this would seem to be due to a fortuitous set of

circumstances. Evidence favors the view that the earth's atmosphere is more generous with good seeing. To attain the benefits of these good images requires a level of telescope and dome design, construction, operation and scheduling that is beyond our current level of practice, but not beyond our current potential.

5. SPECKLE INTERFEROMETRY I. A Test on an Earth Orbital Satellite

S. P. Worden, E. K. Hege, E. N. Hubbard, M. S. Gresham, N. J. Woolf, and P. A. Strittmatter. Air Force Space Division Report (1981)

The astronomical technique known as speckle interferometry shows considerable promise for satellite surveillance and imaging. With speckle interferometry, it is possible to remove image degradation caused by atmospheric turbulence. In this way, resolution on satellite images could be improved by a factor of fifty with existing telescopes. We used this method to determine the size and shape of a high altitude satellite. Without speckle interferometry such information would be impossible to measure. However, to produce routine satellite images we are developing improved computer processing. Even with speckle interferometry we can only marginally resolve high altitude satellites. To provide satisfactory imagery of these objects we need telescopes much larger than existing instruments. To this end, we are working to adapt a large multiple mirror telescope system for speckle interferometry. This telescope is the prototypte for telescopes a factor of ten larger than any now existing.

6. COMPUTER SIMULATIONS OF A PHASE-UNWRAPPING TECHNIQUE IN IMAGING

W. J. Cocke. Unpublished.

A simple phase-unwrapping technique in "blind" deconvolution speckle imaging is tested with two-dimensional computer-simulated data. The output images are cleaned with an iterative Fienup method, and the effects of changing speckle widths between object and point-source calibration are shown to have large effects.

7. COMPUTER SIMULATION COMPARISONS OF SPECKLE IMAGE RECONSTRUCTION TECHNIQUES

W. J. Cocke, Proc. S.P.I.E., 231, 99 (1980).

Two phase retrieval methods are tested with two-dimensional simulated noisy speckle image data: a simple phase unwrapping algorithm and a Knox-Thompson algorithm. These are used in combination with the blind deconvolution and Welter-Worden autocorrelation seeing correction methods. The final images are retouched with the iterative Fienup methods.

8. SPECKLE INTERFEROMETRY AT THE MMT

E. K. Hege, E. N. Hubbard and R. R. Howell.
MMTO Observer's Report (1979).

Successful two-beam optical interferometry (speckle) has been accomplished using the Multiple Mirror Telescope. Observations were made at 6563A with 20A bandpass (α Ori) and 5500A with 100A bandpass (52 Ari). These measurements demonstrate the necessary mechanical integrity of the optical support structure for aperture synthesis optical interferometry.

9. A METHOD FOR PRODUCING SEEING-CORRECT IMAGE AUTOCORRELATION FUNCTIONS AND AN IMAGE RECONSTRUCTION FOR A BINARY STAR.

E. K. Hege, E. N. Hubbard, M. S. Gresham, P. A. Strittmatter, N. J. Woolf and S. P. Worden. Unpublished (1980).

We present a practical method for producing speckle auto-correlation functions self-corrected for seeing effects. The method is applied to the 6.57 magnitude AO visual binary ADS 13449 observed with the 2.3m telescope. The Fienup method for reconstructing images from their Fourier moduli is then used to produce a seeing corrected, aperture resolved image. The observed magnitude difference 0.3m is in agreement with the values 7.0m and 7.3m reported by visual observers. The Fienup method does not, however, resolve the 180° phase ambiguity of the auto-correlation function.

10. TWO-APERTURE SPECKLE INTERFEROMETRY USING THE MULTIPLE MIRROR TELESCOPE.

E. K. Hege, E. N. Hubbard, N. J. Woolf and P. A. Strittmatter. Unpublished (1980).

We report successful two-mirror speckle interferometry at optical bandpasses of 20A at 6560A and 100A at 5500A. The stability of the optical support structure is such that a ± 25 μm interferometric coherence length can be maintained for periods of 20 minutes or more while the telescope tracks an object. Michelson interferometer fringes are shown in the speckle interferometric auto-correlation result for 52 Ari at 5500A. A pupil restoring coherent beam combiner design is proposed.

11. SPECKLE INTERFEROMETRIC OBSERVATIONS OF PALLAS

E. K. Hege, W. J. Cocke, E. Hubbard, M. Gresham, P. A. Strittmatter, R. Radick and S. P. Worden. Bul. Am. Astron. Soc. 12, 509 (1980).

We have used newly developed techniques in speckle interferometry to study the asteroid Pallas. The size and shape of Pallas are known from occultation observations, and its rotational period and pole orientation have been derived from photometric measurements. On 12 and 13 September and 10 November 1979, we obtained over 400,000 high speed (60 sec^{-1}) speckle frames distributed among 10 separate observations. These frames consist of photon events detected with the Steward Obsevatory speckle camera, which consists of an image expander, narrowband interference filter, and four-stage image tube. The data are recorded on video tape using a Plumbicon TV camera. The video tape is processed through a video digitizer and computer system. This system identifies photon events and suppresses ion events and effects of image tube after-glow. Results are analyzed via a correlation scheme to produce diffraction-limited autocorrelation functions of the object under study. Direct analysis of these autocorrelations can produce information about the object's size and shape. Further processing with an iterative Fourier analysis scheme can result in actual diffraction-limited images. We report here a successful observation of Pallas which has been processed in this manner. Our observation resolves the body of the asteroid. In addition, it shows features whose time

evolution agrees with the known rotational period. One possible interpretation of these features is in terms of a secondary body in a close, synchronous orbit about Pallas itself.

12. MORPHOLOGY OF THE TRIPLE QSO PG 1115+08

E. K. Hege, J. R. P. Angel, R. J. Weymann and E. N. Hubbard Nature, 237, 416 (1980).

Sub-arcsecond direct images, obtained under conditions of good seeing with the Multiple Mirror Telescope, show no significant wavelength dependence. This strengthens the inference that the three objects are likely to be images of the same QSO produced by intervening matter acting as a gravitational lens. There is evidence that the brightest component is further resolved at a scale of about 0.5 arc-seconds.

13. "MT-2"

N. J. Woolf and J. R. P. Angel. In Optical and Infrared Telescopes for the 1990's, ed. A. Hewitt, Kitt Peak National Observatory, p.1062 (1980).

MT-2 is designed to be the largest prescision telescope for optical and IR astronomy that can be produced within the size and weight limitations of the current 4 - 5 meter class telescopes. The heart of MT-2 is the production of inexpensive lightweight 5 meter paraboloids in a lightweight cell. This paraboloid would become a basic building block. MT-2 uses 8 of these paraboloids in an MMT-like configuration to give an effective aperture of 14 meters, and angular resolution corresponding to 22 meters maximum separation. An appendix discusses ways of minifying the effects of seeing, self-induced seeing, atmospheric refraction etc.

14. DIFFRACTION PATTERNS AND SIGNAL/NOISE RATIOS FOR POSSIBLE MULTIPLE MIRROR TELESCOPES.

N. J. Woolf, A. B. Meinel and M. Meinel, Optical Science and Optical Engineering, 9, (1982). In press.

We have been studying diffraction patterns, and signal/noise ratios for various possible multiple mirror telescope schemes as constrasted with a single dish. This work is to explore possible configurations for a giant telescope for attaining high resolution images on relatively faint objects (such as satellites in near synchronous orbit). The chief configurations being studied are circles with 6, 7 and 8 mirrors, and a square with 8. Various non-degenerate arrays produce diffraction patterns with very little energy in the central maximum, thus even for speckle work they are likely to produce results with a low signal/noise ratio.

15. "AN INTENSIFIED EVENT-DETECTING TELEVISION SYSTEM FOR ASTRONOMICAL SPECKLE INTERFEROMETRY".

E. K. Hege, E. N. Hubbard and P. A. Strittmatter, Proc. S.P.I.E. 264, 29 (1980).

Abstract: A four-stage electrostatic image intensifier transfer lens coupled to a plumbicon television camera is used both as a photoelectron event-detecting system and as an analogue detector for the Steward speckle camera. The system is capable of continuous logging of photoelectron event data allowing 100 percent utilization of telescope aperture time by use of a Grinnell GMR-27 video digitizer and graphic television display with a special modification for lag-free event detection. Data can be processed on-line at the site or recorded for off-line processing using a standard analogue video recorder. A seeing-

corrected reconstruction of the diffraction limited image derived from the speckle interferometric image autocorrelation computed from 200 television frames of the magnified image of a seventh magnitude close visual binary star observed with the Steward 2.3 meter telescope reported. The system has been applied to speckle interferometry of objects as faint as visual magnitude 16.

16. "THE STEWARD OBSERVATORY SPECKLE INTERFEROMETRY PROGRAM"

P. A. Strittmatter, Proc. S.P.I.E. 243, 75 (1980).

Abstract: The present status of the Steward Observatory speckle interferometer system and the associated reduction and image analysis programs are reviewed. Some recent results on solar system objects and quasars are reported.

17. "POSSIBLE SECONDARIES OF ASTEROIDS FOUND BY SPECKLE INTERFEROMETRY".

E. K. Hege, W. J. Cocke, E. N. Hubbard, J. Christou and R. Radick. Bul. Am. Astr. Soc., 12, 662 (1980).

Abstract: We report speckle interferometric observations of 2 Pallas and 12 Victoria which show evidence for secondary objects. The preliminary results for Pallas previously reported here have been further analyzed and fitted by computer modelling, by a system consisting of the primary object and an unresolved seconday in a close (synchronous?) orbit. This puts the secondary at 2.7 Pallas radii, about 4 magnitudes fainter than Pallas itself.

18. "SPECKLE INTERFEROMETRIC OBSERVATIONS OF THE TRIPLE QSO PG 1115 + 080".

E. K. Hege, E. N. Hubbard, P. A. Strittmatter and S. P. Worden, Astrophys. J. Lett. 248, L1, (1981).

Abstract: Speckle observations of the 16.2 component (A) of PG 1115 + 080 have shown that it is resolved into two components separated by 0.54 arc seconds in PA ~ 20°. The data suggest that the two components are approximately equally bright and are unresolved at the (degraded) speckle resolution of ± 0.15 arc seconds. These results are consistent with those inferred from long exposure images by Hege, et al. (1980) and by Young, et al. (1980). To our knowledge, they represent the first successful application of speckle interferometry techniques in resolving an objects as faint as 16^m.

19. AN IMAGE RECONSTRUCTION FOR CAPELLA WITH THE STEWARD OBSERVAORY/AFGL INTENSIFIED VIDEO SPECKLE INTERFEROMETRY SYSTEM

W. J. Cocke, E. K. Hege, E. N. Hubbard, P. A. Strittmatter and S. P. Worden, In Proc. I.A.U. Colloq. #62, Flagstaff 1981, ed. R. S. Harrington (1982).

Abstract: The Steward Observatory intensified video speckle camera contains a microprocessor drivenantidispersion prism system and shutter, intensified video wide-field acquisition and provides for microprocessor selection of up to 5 narrowband filters and up to 8 microscope objectives. For calibration or focus tests, a reticle or knife-edge may be inserted in the focal plane. The magnified image is amplified by a four stage Varo electrostatic image intensifier and the output is transfer-lens coupled to a Plumbicon television camera. The video output may be processed on-line or recorded for off-line processing later. A video subtraction algorithm implementing in a Grinnell digital imaging system can provide either photoelectron response records for faint objects or background subtracted analogue records for bright objects. The required speckle image power spectra are

computed either directly by Fast Fourier Transform techniques for bright objects or from speckle response addresses for faint objects. The system has been applied successfully to recover binary structures from objects ranging from magnitude 0 Capella to magnitude 15 Pluto/Charon and the magnitude 16 QSO PG 1115 + 080 A. Recent progress towards true image recovery, including a 4 meter diffraction limited image of Capella is described. The data reduction problems and methods are outlined.

20. RECOVERY OF INTENSITY INFORMATION FROM SPECKLE DATA

W. J. Cocke, E. K. Hege, E. N. Hubbard, P. A. Strittmatter S. P. Worden and R. R. Radick, ibid

Abstract: Speckle autocorrelation functions produced by the Worden autocalibration method yield quite accurate values for ρ and σ (Mod 180°). Image stacking methods can resolve the 180 ambiguity. Relative magnitude estimates are more difficult and require formal deconvolution methods. In addition, it is necessary to correct for photon detection characteristics. Intensity ratios can be inferred from power spectra fringe visibility functions or autocorrelation lobe ratios. Unfortunately both methods involve non-linear functions which propagate measurement errors unfavorably. True image reconstruction techniques appear to provide a more reliable method for obtaining accurate magnitude data. Least squares methods are applied to the "cleaned" autocorrelation function to fit both the point spread function of the measurement and the binary star intensity ratio. Image phase information,

accumulated either by the Knox-Thompson method or by a phase following method we have developed, can be used to constrain the Fienup iterative process for reconstructing an image from the "cleaned" power spectrum. Results from these methods are presented and their relative merits and limitations are discussed. Comparisons with lunar occultation results are made.

21. OBSERVED ASYMMETRY IN THE SHAPE OF ALPHA ORIONIS

L. Goldberg, E. K. Hege, E. N. Hubbard, P. A. Strittmatter and W. J. Cocke Second Cambridge Workshop on Cool Stars, Stellar Systems and the Sun, M.S. Giampapa and L. Golub, eds. SAO Special Report 392, p. 131 (1982).

The Steward Observatory intensified video speckle camera (Hubbard, et al. 1979, Hege, et al. 1980) was used at the Steward 2.3 m telescope on 24 Nov 80 and the KPNO 4 m telescope on 3 Feb 81 for observations of Alpha Orionis with a number of interference filters of different passbands and central wavelengths. Preliminary analysis yielded elongated autocorrelation functions, 157° (mod 180°) using 3A at 6563A on 24 November and 28° (mod 180°) using 20A at 6500A on 3 February. Further reductions of the 3 February observation, for which speckle image phases were accumulated, produced an out-of-round figure excess intensity at position angle 208°, the diameter of the major axis being 63 arc ms and that of the minor axis 59 arc ms. The smaller value is in good agreement with measurements by Roddier, et al. (1981) using a rotation shearing interferometer in November 80. The angles of elongation correlate with values inferred from measurement of the linear polarization by Hayes

(1981), who found $\theta = 86^{\circ}$ P = Ø.59% on 3Ø November 198Ø and $\theta = 113^{\circ}$, P = Ø.85% on 1 February 1981. Possible interpretations of the observed asymmetry are discussed.

22. SPECKLE INTERFEROMETRIC OBSERVATIONS OF PLUTO AND CHARON

E. K. Hege, E. N. Hubbard, J. D. Drummond, P. A. Strittmatter, S. P. Worden, T. Lauer, Icarus (1982). In press.

We report speckle interferometric observations of Pluto and its moon Charon obtained on 5 June 1980 with a single 1.8 meter mirror of the Multiple Mirror Telescope. Using a digital television speckle camera which records individual photon arrivals and has a 100% duty cycle, we obtained good results in 28 minutes observation time. We used an autocorrelation/cross correlation subtraction scheme together with deconvolution by a similarly observed point source to calibrate our results. We report a separation of Ø.31 (Ø.Ø5) between Pluto and Charon at position angle 285° (7°) for JD 2444395.75. This result and other direct observations indicate that an adjustment of -4.Ø hours to the orbital epoch is required. Our observation, the first resolution of the system near minimum separation, suggests that the inclination of the orbit to the plane of the sky should be increased by 3°, which will delay the onset of the predicted eclipse season by one apparition. Our data is consistent with Pluto diameter Ø.14 (±Ø.Ø2) = 3ØØØ (±4ØØ) km and Charon diameter Ø.Ø5 (±Ø.Ø3) = 11ØØ (±6ØØ) km. We have reanalyzed Arnold et al. (1979), Ap. J. (Letters), 234, L159) speckle results and believe that they show the effects of Charon rather than only surface structure as reported in that paper.

23. THE STEWARD OBSERVATORY SPECKLE INTERFEROMETRY SYSTEM

E. K. Hege, E. N. Hubbard, P. A. Strittmatter and W. J. Cocke
Optica Acta (1982). In press.

An intensified video camera with digital video readout has been implemented for use with the Steward Observatory speckle camera. Video subtraction algorithms implemented in a Grinnell digital television system can provide either photoelectron response records for faint objects or background subtracted analogue records for bright objects. The required speckle image power spectra are computed indirectly from the autocorrelation functions accumulated from the event address lists produced for faint objects or directly by Fast Fourier Transform techniques from the analogue data for bright objects. Methods for producing properly deconvolved, noise bias corrected power spectra have been developed. The system has been applied successfully to recover high resolution images for objects ranging from magnitude 0 Capella to the magnitude 16 QSO PG1115+080A.

24. SPECKLE INTERFEROMETRIC IMAGES OF BINARY STARS WITH PHASE RETRIEVAL BY BATES' ALGORITHM

W. G. Bagnuolo and E. K. Hege, Unpublished.

Speckle interferometric observations of Capella have been analyzed by means of an algorithm similar to that used by Bates, et al. (1978) and Bates and Cody (1980). The results indicate ρ = 0.0414 (±0.010), $\theta = 153^{\circ}$ (±0.6), m = 0.445 (±0.032) in good agreement with the analysis of Cocke, et al. (1982) but larger than the intensity ratio inferred by spectroscopic analysis by Wright (1954).

25. SUCCESSFUL EFFORTS TO RECONSTRUCT A PHASED MMT PUPIL

D. McCarthy, P. Strittmatter, K. Hege, J. Drummond, N. Woolf, F. Low, MMTO Observers' Report (1981)

We report phased operation of each of the three pairs of opposite mirrors at optical wavelengths (550 nm to 750 nm) demonstrating the successful operation of an instrument to reconstruct an adequately coherent MMT pupil over a wide field. The interferometer was used to measure the diameter of α Tau at 750 nm. The result, 23.6 (±1.8) agrees favorably with 23.1 and 22.2 obtained by Radick and Africano (1981).

26. THE MMT AS AN OPTICAL-INFRARED INTERFEROMETER AND PHASED ARRAY

D. W. McCarthy, P. A. Strittmatter, F. J. Low and E. K. Hege
In Proc. S.P.I.E., 332, (1982).

Large gains in spatial resolution can be achieved by operating the 6.9 m MMT in equal-pathlength configurations containing two or more telescopes. At present, pathlengths from radially opposite telescopes are equalized routinely at wavelengths of ~ 0.5 um and 5.0 um. Measurements of the resulting Michelson fringes have characterized pathlength stability versus elevation angle, temperature, and perturbations of the optical elements. Effects of telescope pointing and tracking have also been measured. As a fully phased array, the MMT acts as an unfilled aperture to avoid some effects of atmospheric seeing while still responding to most of the spatial frequencies present in a filled 6.9m aperture. Instrumental designs have been developed to reconstruct a fully phased MMT pupil for joint scientific applications at optical and infrared wavelengths. Such designs must possess low infrared emissivity,

must compensate for the polarization changes caused by non-normal reflections in the telescopes, and must eliminate the inclination of wavefronts produced by the standard beam-combining optics.

27. SPECKLE INTERFEROMETRY II

S. P. Worden, E. K. Hege, E. N. Hubbard and P. A. Strittmatter
Air Force Space Division Report (1982). In press.

We present a review of speckle interferometry, including current status and results. In section I we provide a background of the Fourier mathematics used in image processing and optical systems. In section II we describe how the atmosphere degrades astronomical images and how speckle interferometry has been used to recover high resolution detail. In section III we describe new work to recover actual optics-limited images. Active optics systems are reviewed and compared with speckle interferometry. Recent work indicates that large telescope optics limited images are recoverable for objects as faint as +15 stellar magnitudes.

28. IMAGE SHRINKING IN SUB-ARC SECOND SEEING AT THE MMT and 2.3m TELESCOPE

N. J. Woolf, D. W. McCarthy and J. R. P. Angel
In Proc. S.P.I.E. 332 (1982).

Observations of image size and motion have been made at the MMT and 2.3m telescopes. At the 2.3m, simultaneous observations were made of image size and position at 0.8 μm and various IR wavelengths. The MMT observations were all at 0.6 μm, and were used to measure the isoplanicity of the atmosphere for image motion, the time development of image position, and the telescope to telescope correlation of image motion. At both telescopes the image size was larger than expected for the image motion. The

MMT results showed that although there is a finite outer scale of turbulence for the atmosphere, it did not appreciably reduce image motion. Therefore, the excess image size is caused by excess small scale turbulence (presumably inside the dome), together with various telescope imperfections. It is inferred that sub-arc second seeing is frequently available at both Mt. Hopkins and Kitt Peak, but that the image is substantially deteriorated in the observations. While correction for image motion is a necessary part of a program to shrink telescopic images, there are other high priority cures also needed.

VIII. Speckle Interferometry Software: Summary of Programs For Data Reductions and Image Analysis

Data processing is accomplished in two environments, the Steward Observatory minicomputer systems and the University of Arizona Cyber 175/DEC-10 systems.

VIII.A. MINICOMPUTER SYSTEMS

This environment hosts the primary digital video detection processes summarized conceptually in FigureII.2. This system consists of the primary speckle detector (D), the video-subtracting digitizer (S), and the logical and computational subsystems (L) linked by video analogue channels (V_1 and V_2). The Grinnell GMR-27 video analogue-to-digital conversion and digital video memory system, with specially designed video subtraction capability (S), is the primary video processing element of the system. The video difference may be output in digital format for on-line processing by Digital Logic I and/or as video analogue for later off-line processing, in which case it must subsequently be redigitized.

The provision for video analogue recording (V_1 and V_2) gives considerable flexibility in implementing this system at various observing sites which may or may not have video subtractor (S) and/or logic processors/computers (L) available for use at the telescope. Video tape recording (VTR) provides the most convenient, most compact and cheapest currently available archival medium for the primary speckle interferometric data base in order to enable subsequent processing and/or reprocessing of

the data. The bandpass limitation of the VTR does not preclude its use in speckle interferometry, although in some applications there may be a significant loss of speckle resolution.

The actual functions of Digital Logic I and II, necessary to implement event-detection and analogue data compression algorithms, to produce on-line ACF and LE images and to log analogue and event address lists for further processing are presently implemented in software using the combined hardware and software capabilities of the GMR-27 and EDS.4 image processing minicomputer system. A hardware realization of the event-detecting Digital Logic I and its associated buffers for real-time on-line processing is presently under construction.

The preliminary implementation of Digital Logic I in software has permittted several experimental algorithms to be easily tested. The possibility of localizing detected photoelectrons to a unique pixel is of particular interest. Initially the hardware device to localize events to a single pixel along a single along a single scan line is being implemented as a version of Digital Logic I. The feasibility of several two-dimensional event-centroiding algorithms has been successfully demonstrated with software post-processors of the "significant-pixel" detector output.

The acutal software modules are summarized in Table VIII.I.

VIII.B. THE CYBER 175/DEC-10 SYSTEMS

Systems exist for the processing of both analogue-mode and event-mode data to achieve the reductions implied by the discussions above and represented schematically in Figure VIII.1.

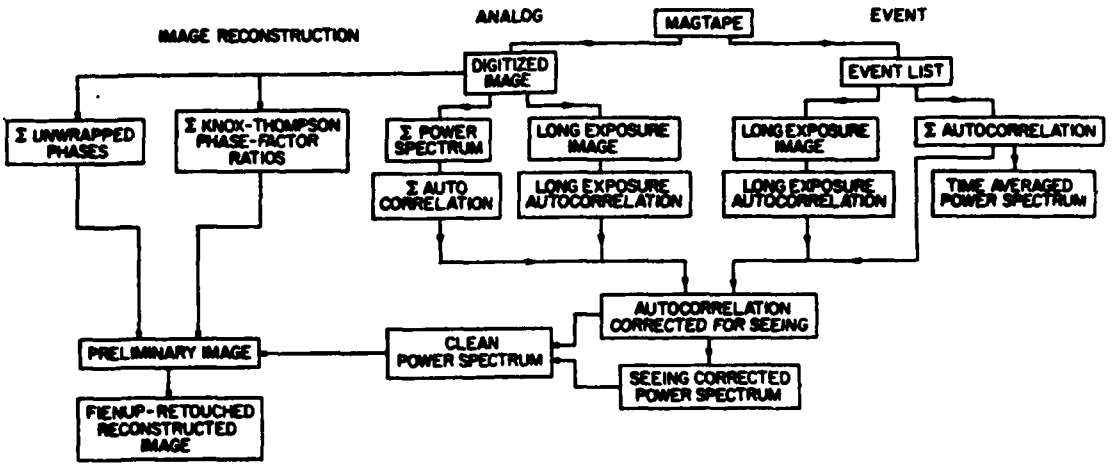

Figure VIII.1. Summary of data reductions processes. Digitized video data, event mode or analogue mode is written on 9-track magtape. Four intermediate results are produced for either data mode. These are used to produce an autocorrelation function and power spectrum corrected for seeing which are then subjected to an ierative procedure to produce a clean power spectrum. Analogue data can also be processed to accumulate image phase information, which when combined with the clean power spectrum produces a preliminary estimate. This estimate may be subjected to iteration by the Fienup algorithm to produce a reconstructed image.

The actual software modules for realizing the functions diagrammed in Figure VIII.1 are summarized in Table VIII.II.

VIII.C. IMAGE ANALYSIS AND INTERPRETATION

The final image analysis and interpretation is accomplished in a interactive image processing environment realized with the Steward Observatory Eclipse/Grinnell/Array processor minicomputer system. The necessary image analysis capabilities are included in the package analysis also listed in Table VIII.1.

Further details, including program listings, are available from the authors.

TABLE VIII.I

SOFTWARE (FORTH)

DATA GENERAL NOVA (POINT 4) AND ECLIPSE

Vocabulary Name	Purpose
EVENT	The event digitizer system logs address of pixels whose values exceed a specified threshold and writes them on 9-track magtape 800 BPI for Cyber processing by SPEKLPH.
ANALOG	Captures analog data in a compressed format. 2 x 2 cells in the original 240 x 256 video field averaged to 8-bit precision in a 120 x 128 analogue data raster or a 128 x 128 sub-field are written on 9-track magtape 800 BPI for Cyber processing by PHASE.
ANALYSIS	Interactive video analysis package for interactive use with the Grinnell Image Memory/Display and image files on the minicomputer system. Reads tapes produced by Cyber processors. Vector and array arithmetic for acquiring and processing one-dimensional cuts and for two-dimensional least-squares function fitting routines (Jeffreys, 1980).
PEAK-FINDER	Integrates direct video imaging with integration-to-integration image centroiding to remove guiding and tracking errors in order to produce seeing limited long-exposure images. Integrations from 1 video frame to arbitrary duration are programmable (Hege et al. 1980). Can operate in either analogue or event-detecting mode.

TABLE VIII.II

SOFTWARE (FORTRAN/COMPASS)

CYBER 175/DEC 10

File Name	Purpose
SPEKLPH	The event address data processor. Computes averaged power spectra, long-exposure image, long exposure power-spectrum and autocorrelation function, averaged auto-correlation functions and seeing corrected autocorrelation function (modified Welter-Worden). Produces FORTH readable output on 9-track magtape 800 BPI. Has event-centroiding option.
SPEDIT	Plots reduced versions of individual speckle analogue data frames on line printer, for editing prior to input to PHASE.
PHASE	The analogue data processors. Computes averaged power spectra, unwrapped phase angles, phase factor ratios, and long-exposure image.
PRECON	Processes power spectra by deconvolving, filtering an/or "cleaning".
WORSUB	Does seeing self-correction (refined Welter-Worden subtraction).
FINUP	Combines processed power spectra and phases for trial image and then does Fienup retouching.
DPROJ	Does 1-D projections of power spectra for computing double-star parameters.
DSLAST	Finds double-star parameters (including intensity ratios) from autocorrelations (does PSF fitting).
GRN256	Makes FORTH-readable tapes of images, power spectra, etc., for viewing on Grinnell and for further processing by Steward computers.
MOON	Makes images, autocorrelations, power spectra of speroids illuminated at arbritrary phase angles. Used for asteroid image modelling and simulation studies.
SPEKL26	Generates photographic hardcopy of image output using the Dicomed (IPPS) facility at KPNO.

SPEKL24 — A general purpose image processing macrocompute. Used for simulations, generalized array processing, FFT's etc.

There are also miscellaneous auxiliary files of supporting software.

IX. Acknowledgements

In addition to the co-authors, many other people contributed to this project. The work would not have originated, nor would it have continued, without the encouragement and support of Capt. S. P. Worden. We especially thank Gene Hubbard who contributed to the project from its beginning until the completion of his Ph.D. in 1981. John Cocke made substantial contributions in implementation of image reconstruction algorithms. We are also grateful to Richard Radick for substantial critical review of the draft of the manuscript as well as continuing discussions throughout the later stages of the work.

The following students and technical staff also made significant contributions:

Students	Engineering and Technical Staff
J. Christou	D. Young
M. Gresham	T. Sargent
J. Freeman	J. Rill
D. Rautenkranz	B. Macklin
W. Wisniewski	

X. References

1. Bagnuolo, W. G., In Proc. IAU. Colloq. 62, Flagstaff, 1981, R. S. Harrington, Ed. (1982).

2. Christy, J. W. and Harrington, R. S., Astron. J. 83, 1005 (1978).

3. Cocke, W. J., Proc. Soc. Photo-Opt. Instr. Eng., 231, 99 (1980).

4. Dainty, J. C., Mon. Not. R. Astr. Soc., 169, 631 (1974).

5. Dainty, J. C., "Stellar Speckle Interferometry", Laser Speckle and Related Phenomena, J. C. Dainty, Ed., p. 255 (Springer-Verlag, 1975).

6. Dainty, J. C., Mon. Not. R. Astr. Soc., 183, 223 (1978).

7. Fienup, J. R., Optics Lett., 3, 27 (1978).

8. Fienup, J. R., Opt. Enging., 18, 529 (1979).

9. Fienup, J. R., Feldkamp, G. B, Proc. Soc. Photo-Opt. Instr. Eng. 243, 95 (1980).

10. Frost, R. L., Rushforth, C. K., and Baxter, B., AFOSR Technical Report UTEC 79-081, (1979).

11. Gezari, D. Y., Labeyrie, A., Statchnik, R. V., Astrophys. J., 173, L1 (1972).

12. Goldberg, L., Hege, E. K., Hubbard, E. N., Strittmatter, P. A., Cocke, W. J., Second Cambridge Workshop on Cool Stars, Stellar Systems and the Sun, M. S. Giampapa and L. Golub, Eds. SAO Special Report 392, p. 131 (1982).

13. Hayes, D. P., Astrophys. J., Lett. in press (1982).

14. Hege, E. K., Hubbard, E. N., Strittmatter, P. A., Proc. Soc. Photo-Opt. Instr. Eng., 264, 29(1980a).

15. Hege, E. K., Cocke, W. J., Hubbard, E. N., Gresham, M., Strittmatter, P. A., Bull. Am. Astron. Soc., 12, 509 (1980b).

16. Hege, E. K., Cocke, W. J., Hubbard, E. N., Christou, J., Radick, R. R., ibid, 662 (1980c).

17. Hege, E. K., Hubbard, E. N., Strittmatter, P. A., Worden, S. P., Astrophys. J., 248, L1 (1981).

18. Hege, E. K., Hubbard, E. N., Strittmatter, P. A., Cocke, W. J., Optica Acta (1982). In press.

19. Hege, E. K., Hubbard, E. N., Drummond, J. D., Strittmatter, P. A., Worden, S. P., Lauer, T., Icarus, (1982). In press.

20. Hubbard, E. N., Hege, E. K., Reed, M. A., Strittmatter, P. A., Worden, S.P., Astron. J., 84, 1437 (1979).

21. Jefferys, W. H., Astron. J., 85, 177 (1980).

22. Knox, K. T., Thompson, B. J., Astrophys, J. (Lett.), 193, L45 (1974).

23. Labeyrie. A., Astron. and Astrophys. 6, 85 (1970).

24. Labeyrie. A., Ann. Rev. Astron. Astrophys. 16, 77 (1978).

25. Michelson, A. A., Pease, F. G., Astrophys. J., 53, 249 (1921).

26. McAlister, H. A., Astron. J., 86, 795 (1981).

27. Mertz, L. N., Applied Optics, 18, 611 (1979).

28. Papaliolios, C., private communication.

29. Radick, R. R. and Africano, J. L., Astron. J., 86, 906 (1981).

30. Weymann, R. J., Latham, D., Angel, J. R. P., Green, R. F., Liebert, J. W., Turnshek, D. A., Turnshek, D. E., Tyson, J. A., Nature, 285, 641 (1980).

31. Woolf, N., Pub. Astron. Soc. Pacific, 91, 523 (1979).

32. Worden, S. P., Stein, M. K., Astron. J., 84, 140 (1979).

33. Worden, S. P., Hege, E. K., Hubbard, E. N., Woolf, N. J., Strittmatter, P. A., Air Force Space Division Report (1981).

34. Worden, S. P., Hege, E. K., Hubbard, E. N., Strittmatter, P. A., Air Force Space Division Report (1982).

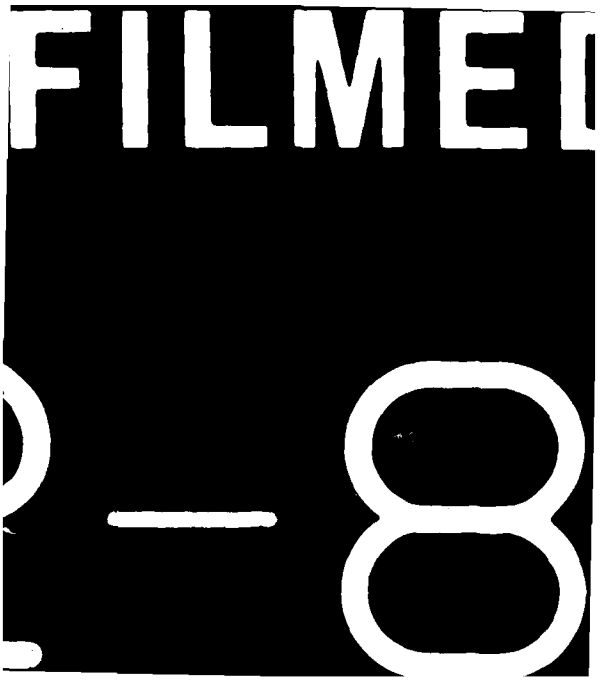
FILME
-8